POLITECNICO DI TORINO
Repository ISTITUZIONALE

On the Uplink Performance of Cooperative LEO Satellite Networks Under Realistic Assumptions

Original
On the Uplink Performance of Cooperative LEO Satellite Networks Under Realistic Assumptions / Ben Salem, H., Behrooz, M., Tarable, A.. - In: IEEE ACCESS. - ISSN 2169-3536. - 14:(2026), pp. 80893-80911. [10.1109/ACCESS.2026.3694958]

Availability:
This version is available at: 11583/3015297 since: 2026-09-08T19:57:51Z

Publisher:
IEEE

Published
DOI:10.1109/ACCESS.2026.3694958

Terms of use:

This article is made available under terms and conditions as specified in the corresponding bibliographic description in the repository

Publisher copyright

(Article begins on next page)

28 October 2026

IEEE Access
Multidisciplinary ⋮ Rapid Review ⋮ Open Access Journal

Received 8 April 2026, accepted 11 May 2026, date of publication 19 May 2026, date of current version 29 May 2026.

Digital Object Identifier 10.1109/ACCESS.2026.3694958

APPLIED RESEARCH

On the Uplink Performance of Cooperative LEO Satellite Networks Under Realistic Assumptions

HOUCEM BEN SALEM[1,2], BEHROOZ MAKKI[1], (Senior Member, IEEE), AND ALBERTO TARABLE[3], (Member, IEEE)

[1]Ericsson Research, Ericsson, 417 56 Gothenburg, Sweden
[2]Politecnico di Torino, 10129 Turin, Italy
[3]IEIIT, Consiglio Nazionale delle Ricerche, 10129 Turin, Italy

Corresponding author: Houcem Ben Salem (houcem.bensalem@polito.it)

Funded by the European Union, under ANTERRA 101072363 HORIZON-Marie Skłodowska-Curie Actions (MSCA)-2021-Doctoral Network(DN)-01. Views and opinions expressed are however those of the authors only and do not necessarily reflect those of the European Union. Neither the European Union nor the granting authority can be held responsible for them.

ABSTRACT In this paper, we investigate the uplink performance of Low-Earth Orbit (LEO) satellite constellations, focusing on the role of Inter-Satellite Links (ISLs) in enhancing communication performance. The study examines two configurations of the proposed Soft Handover (SH) strategy: 1) Single-Satellite Relay (SSR), where one target satellite assists the serving satellite, and 2) Multi-Satellite Relay (MSR), where multiple satellites cooperatively forward the received signal from ground user (GU) through ISLs to the serving satellite. The results obtained under SH are compared with those from conventional Hard Handover (HH) schemes. Using realistic 3GPP channel models for both ground-to-satellite (G2S) and ISL, we derive a framework based on information theory to estimate the system block error rate (BLER) and conditional capacity, employing two relaying techniques: Amplify-and-Forward (AF) and Decode-and-Forward (DF). We also compare the impact of using Maximal Ratio Combining (MRC) and Selection Combining (SC) to aggregate the signals received from the GU and the relaying satellites at the serving satellite. Furthermore, we investigate the impact of imperfect Channel State Information (CSI) and beam misalignment within ISLs and propose mitigation techniques to counteract these effects. Our analysis demonstrates that the proposed SH scheme—under both SSR and MSR reception—significantly outperforms traditional HH methods, reducing the required signal-to-noise ratio (SNR) on the G2S link and the required transmission power on the ISL to meet given quality-of-service requirements. For instance, a constellation comprising 100 LEO satellites requires an SNR of 21.5 dB to achieve a BLER of 10^{-4} with HH, whereas the proposed SH approach achieves the same BLER with only 12 dB. These results highlight the effectiveness of the proposed SH techniques in improving the robustness and efficiency of future LEO satellite communication networks.

INDEX TERMS LEO satellite networks, non-terrestrial networks, soft handover, relay-assisted communications, inter-satellite link.

I. INTRODUCTION

Next-generation wireless telecommunication systems aim to support an unprecedented traffic volume while ensuring reliable and ubiquitous connectivity. However, terrestrial networks face spectrum scarcity and coverage limitations, particularly in remote areas or during disaster relief operations. To address these challenges, Non-Terrestrial Networks (NTNs), including satellites, autonomous aerial vehicles (AAVs), and high-altitude platforms (HAPs), have emerged as a promising solution [1], [2]. Among these, Low-Earth Orbit (LEO) satellites currently represent the most attractive option, offering wide coverage compared to AAVs and HAPs, and significantly lower latency (round-trip times around 30 ms) than Middle-Earth Orbit (MEO) and Geostationary-Earth Orbit (GEO) systems, while also reducing deployment costs.

LEO satellite networks present unique challenges due to their low orbital altitude. A single LEO satellite covers a limited geographical area, requiring large constellations to

The associate editor coordinating the review of this manuscript and approving it for publication was Abbas Kiani.

© 2026 The Authors. This work is licensed under a Creative Commons Attribution 4.0 License.
For more information, see https://creativecommons.org/licenses/by/4.0/

ensure global coverage. Moreover, the high orbital velocity leads to short visibility periods: for example, a satellite at 550 km altitude completes one orbit in approximately 1.6 hours and remains visible to a Ground User (GU) for only a few minutes. This results in frequent handovers and rapidly varying channel conditions. In addition, the ground-to-satellite (G2S) link must maintain reliability despite elevation-dependent propagation effects and atmospheric variations encountered during a satellite pass. Therefore, robust G2S modeling [3] and efficient handover strategies [4], [5] are essential to ensure seamless connectivity and optimal performance in such a rapidly changing environment.

The G2S link is studied, for example, in [6], [7], [8], [9], [10], [11], [12], [13], [14], [15], [16], [17], [18], [19], [20], [21], [22], [23], [24], [25], [26], [27], [28], [29], and [30], where different statistical models have been proposed to capture the dynamic nature of signal behavior and the propagation environment. A widely adopted reference is the Loo-based LMS model in [6], which assumes a predominant LoS component affected by log-normal shadowing and a Rayleigh-distributed multipath term; this model has been embedded into one-state [6], [7], [8], [9], [10], two-state [11], [12], [13], [14], and multi-state Markov or semi-Markov frameworks [12], [15], [16], [17], [18], [19], [20], [21], [22], [23], [24], [25], [26], [27], [28], [29], [30], [31] to better represent transitions between good and bad propagation conditions. These multi-state LMS models offer a physically intuitive description of blockage dynamics and elevation-dependent attenuation, but are typically applied to static geometries or single snapshots, without explicitly tracking the continuous temporal evolution of performance metrics such as the Block Error Rate (BLER) over a complete satellite pass, where elevation angles and path conditions vary rapidly.

Handover protocols in LEO satellite networks largely depend on the underlying architectural design. For cell management, two primary approaches are typically considered [4], [32]: the *Earth-fixed cell*, where a satellite dynamically steers its antennas to maintain continuous coverage over a specific ground area, and the *Earth-moving cell*, in which the beam footprint follows the satellite along its orbit. The latter poses greater challenges for handover management but simplifies antenna design.

Focusing on link-layer handovers in LEO systems, three main categories can be identified [33], [34]: *spot-beam handover*, *satellite handover*, and *inter-satellite link (ISL) handover*. Beam handover occurs when the GU is transferred between two beams of the same multibeam satellite [35]. In Earth-moving beam systems, such handovers are frequent due to the small coverage area of each beam and the relative motion between the satellite and the GU. Conversely, in Earth-fixed beam systems, beam handovers occur less often. Satellite handover takes place when the GU connects to a different satellite. Although less frequent, this type of handover is more complex and is essential for maintaining long-duration connectivity according to various criteria [36], [37], [38]. ISL handovers, on the other hand, occur not only due to technical interruptions or link shutdowns but also as a natural consequence of satellite motion, which causes satellites to drift out of each other's LoS or communication range. In such cases, ongoing ISL-based communications must be rerouted accordingly [39]. In the following, we consider Earth-fixed cells and adopt a *Hybrid Wide-Spot Beam* (HWSB) coverage scheme [40], [41]. Unlike the conventional spot-beam approach—where beam footprints on Earth move with the satellite trajectory—the HWSB scheme enables narrowband spot beams to be dynamically directed toward GUs, thereby eliminating the need for beam handovers.

Suppose that a GU is connected to a serving satellite. Typically, handover decisions are managed by the network control center. Before the handover occurs, various strategies can be employed to identify the target satellite that will serve the GU afterward. A simple selection rule is for the GU to connect to the closest satellite [42]. Alternatively, the target satellite can be chosen based on maximum visibility time [38] or minimum traffic load [37]. Regardless of the selection method, two main handover scenarios exist: Hard Handover (HH) and Soft Handover (SH).

In the HH scenario, the GU maintains a connection with only one satellite at a time. When a handover occurs, the GU first disconnects from the current serving satellite before establishing a new link with the target satellite, following a break-before-make procedure. This introduces service interruption risks and handover failures, particularly in LEO systems with frequent satellite transitions. While this single-link approach simplifies network management, it may suffer from poor channel conditions and consequent quality-of-service degradation, since it does not exploit the spatial diversity offered by the typically many satellites simultaneously visible from the GU. For this reason, we propose a SH framework, which enables multiple satellites to receive and relay the uplink signal of the GU, thereby significantly enhancing reliability through spatial diversity. This is achieved by leveraging ISLs [43], [44], [45], [46], [47], [48], which enable a cooperative LEO network where relay satellites forward the GU's received signal to the serving satellite (which is assumed to be the satellite with the highest elevation) through realistic ISL channels that incorporates practical impairments, including pointing misalignment, range-dependent attenuation, and finite link capacity.

We introduce two SH architectures: SH-SSR (Single-Satellite Relay) where one neighbor satellite relays to the serving satellite, extending prior ISL-based studies with more realistic channel modeling; and SH-MSR (Multi-Satellite Relay) where all visible satellites beyond the serving satellite cooperatively relay, exploiting full constellation diversity unavailable with no relaying or single-relay schemes. Post-transition, the former serving satellite continues to act as a relay, ensuring continuity of diversity throughout the entire satellite pass. Unlike prior works that assume static geometry

and ideal ISLs, our proposed dynamic SH-MSR framework explicitly captures time-varying satellite visibility and quantifies the impact of practical impairments, particularly pointing misalignment, on cooperative reception performance.

In [49], a sophisticated algorithm is developed in which a finite time horizon is considered in the future, instead of only the current time, based on the predictable trajectories of the LEO satellites. In [50], the authors study mapping a set of GUs into a LEO constellation based on network flow maximization. Other works suggest the use of reinforcement learning (RL) [40], [51], [52] to determine a handover strategy defining a reward for a given action, so that the system learns how to choose the action with the highest reward. In general, existing SH studies, are primarily limited to SSR. By restricting cooperation to just one relaying satellite, these works fail to exploit the full spatial diversity available in dense constellations. Furthermore, RL-based handover optimization approaches focus on decision-making logic without explicitly quantifying the physical-layer reliability gains achievable through MSR.

Regarding multi-satellite connection to GUs, it is typically known as satellite Multiple-Input Multiple-Output (MIMO) or multi-satellite cooperative networks. After the seminal work in [53], the work in [54] deals with the application of MIMO LoS to the downlink of multibeam GEO satellite communication systems. In [55], the downlink of a feeder link with two LEO satellites and a uniform circular array at the ground station is analyzed in an Additive White Gaussian Noise (AWGN) channel model. Massive MIMO is first introduced for LEO communications in [56] for a single satellite, while [57] proposes an Orthogonal Frequency-Division Multiplexing (OFDM) based downlink design of a LEO network, where four satellites serve each GU. In [58], a joint optimization of hybrid beamforming in the satellites and GUs scheduling is proposed for an architecture in which a given GU can be served by multiple LEO satellites. The channel used in [58] derives from the GOOD state of the channel in [59], which is also the one used in this paper.

These prior works analyze the diversity gains of cooperation, and propose joint optimization for hybrid beamforming. However, they typically rely on idealized assumptions, such as static channel realizations and error-free, infinite-capacity ISLs. The effects of ISL misalignment, range-dependent attenuation, and imperfect Channel State Information (CSI) are generally neglected, which leads to overestimated achievable performance. Consequently, they fail to show how MSR performs under realistic uplink settings, leaving a significant gap in understanding the trade-off between constellation cooperation and link impairments.

In summary, the state-of-the-art exhibits three distinct gaps: (1) G2S models are rarely integrated into dynamic, full-orbit handover analyses; (2) Handover strategies are often limited to single-relay architectures, ignoring the diversity of larger constellations; and (3) MSR studies predominantly assume ideal ISLs, failing to address critical impairments like pointing errors. Our work overcomes these gaps by modeling a comprehensive SH-MSR framework that integrates realistic ITU-R P.681 dynamic channels with a physical ISL model accounting for misalignment and finite capacity, thereby providing a robust assessment of uplink reliability lacking in prior art.

A. CONTRIBUTION OF THIS WORK

This paper investigates a constellation of satellites in a single LEO orbit implementing SH strategies. The main objective is to demonstrate the effectiveness of MSR and advanced signal processing in enhancing the uplink performance of LEO communication systems. The analysis focuses on user-level performance, while system-level optimization is left for future work. Particular attention is devoted to the role of ISLs in enabling efficient signal combining across satellites. A detailed comparison between the proposed SH-MSR approach and conventional HH and SH-SSR schemes highlights the significant performance gains achievable through MSR cooperation. The main contributions of this paper are summarized as follows:

- We model the uplink of a LEO satellite communication system based on MSR, where multiple satellites assist a serving satellite through ISLs to enhance the G2S uplink performance.
- We derive a framework based on information theory, in order to assess the performance of the proposed SSR/MSR strategies in terms of BLER. This method allows us to obtain some theoretical results in specific conditions, allowing us to quantify the impact of channel estimation errors and pilot power allocation without computationally prohibitive simulations.
- We develop a comprehensive Monte-Carlo simulation-based evaluation of the proposed system, where we demonstrate that MSR reception provides substantial diversity and power gains: for a constellation of 100 satellites, the SH-MSR scheme achieves up to 10–12 dB reduction in required SNR compared to HH, and 5–6 dB improvement over SH-SSR reception at a target BLER of 10^{-4}.
- We quantify by simulation the impact of key system parameters—including satellite constellation size, relay transmit power, misalignment variance, and minimum elevation angle)—on achievable BLER performance, revealing optimal trade-offs between constellation density, power efficiency, and link reliability.
- We analyze two different relaying strategies on the relay satellites, namely Amplify-and-Forward (AF) and Decode-and-Forward (DF), with performance evaluated in terms of BLER.
- We investigate the effect of ISL misalignment, showing that optical links at 193 THz are highly sensitive, whereas lower-frequency ISLs (e.g., 2 THz) achieve comparable performance while offering up to 35× greater tolerance to pointing errors, demonstrating the robustness of MSR reception under realistic conditions.

- We study the effect of imperfect CSI, showing that the SH strategy is robust under such conditions, with both SSR and MSR still outperforming HH in different scenarios.
- We compare two different receiver techniques, Maximal Ratio Combining (MRC) and Selection Combining (SC) techniques, showing that MRC offers additional gain at low BLERs, confirming its efficiency for coherent multi-branch combining.
- We discuss the complexity of SSR/MSR in terms of computation and allocation of resources, the implementation issues related to the proposed multi-satellite reception scheme, and some aspects related to the extension to the multiuser scenario.

The proposed SH-MSR scheme shows that multi-satellite cooperation through ISLs can deliver substantial uplink gains. This line of work started with our conference paper [43], where we first assessed the feasibility of using a single assisting satellite—mainly to understand whether an ISL can realistically help the serving satellite during transition. In the present paper, we then formalize and strengthen this concept into a rigorous SSR baseline, including pilot-assisted channel estimation and imperfect CSI, and extending the receiver processing with MRC vs. lower-complexity SC supported by an information-theoretic framework for BLER computation. Building on this validated SSR foundation, we finally develop the new MSR architecture, where multiple visible satellites cooperate simultaneously—enabling a complete, parameter-driven study of ISL benefits and limitations (constellation size, relay power, misalignment, elevation constraints, and CSI accuracy) on the achieved uplink BLER.

Simulations are conducted in a dynamic environment representative of LEO communications. The G2S link model, which accounts for both shadowing and fading effects, follows ITU Recommendation P.681-11 [59], while the ISL model adopts the approach proposed in [44], incorporating antenna pointing errors, range-dependent attenuation, and finite link capacity. Our results demonstrate that the MRC scheme provides substantial gains over SC, confirming its effectiveness as a key enabler for reliable SH operation. For instance, in a constellation of 100 satellites with a reference SNR of 8 dB on the G2S link and a minimum elevation angle of $\delta_{\min} = 10°$, the SH-MSR technique achieves a BLER of 2.9×10^{-6}, compared to 1.4×10^{-2} with SC reception and 7.3×10^{-2} under HH. Similarly, at a reference SNR of 5 dB and a transmitted power of 20 dB W on the G2S link with $\delta_{\min} = 37.5°$, SH-MSR attains a BLER of 7.8×10^{-3}, while SC and HH reach 3.3×10^{-2} and 1.2×10^{-1}, respectively. These results indicate that SH-MSR enables significant power savings and improved link reliability compared to conventional HH without relaying and SC, highlighting its potential for next-generation LEO satellite networks.

B. OUTLINE

The remainder of this paper is organized as follows. In Section II, we describe the system and channel models, detailing the geometrical configuration of the LEO satellite constellation and the propagation characteristics of both G2S and ISLs. Section III specifies the proposed SH framework, including the signal model, the AF and DF relaying strategies, and the combining techniques employed at the serving satellite under both perfect and imperfect CSI. Section IV, we present the analytical derivation of the BLER, highlighting the performance differences between the proposed SH strategies and the conventional HH approach. Section V provides extensive simulation results that validate the analytical findings and examine the influence of system parameters such as constellation size, relay satellite transmission power, minimum elevation angle, misalignment impact on the ISL, and CSI accuracy. Section VI discusses some aspects related to complexity, implementation issues and extension to a multiuser scenario. Finally, Section VII concludes the paper and outlines future research directions.

II. SYSTEM MODEL

In this section, we describe the main model assumptions. In particular, Subsection II-A defines the geometrical model, while Subsections II-B1 and II-B2 introduce the models for the G2S and ISL channels, respectively. Each subsection is accompanied by a notation table.

A. GEOMETRICAL MODEL

We consider a constellation of N_{Sat} satellites deployed in a circular orbit at altitude h_0 above the Earth's surface, with orbital inclination i_{K} relative to the equatorial plane. The satellites are uniformly distributed along the orbit, with angular separation $\alpha_0 = \frac{2\pi}{N_{\text{Sat}}}$ radians, as illustrated in Fig. 1. According to Kepler's laws and [60], the angular velocity of each satellite is

$$\omega = \sqrt{\frac{\mu}{(R_E + h_0)^3}} \quad [\text{rad/s}], \tag{1}$$

where $R_E = 6371$ km is the Earth's mean radius, and $\mu = GM_{\oplus} = 3.986 \times 10^5\ \text{km}^3\text{s}^{-2}$ is the geocentric gravitational constant, with G denoting the gravitational constant and $M_{\oplus}$ the Earth's mass.

The angular position of satellite $\ell \in \{1, \ldots, N_{\text{Sat}}\}$ at time t is

$$\alpha_\ell(t) = \omega t + \alpha_\ell(0). \tag{2}$$

Let $\lambda_\ell(t)$ and $\phi_\ell(t)$ denote the latitude and longitude, respectively, of the sub-satellite point (SSP)[1] at time t. By geometric relations,

$$\lambda_\ell(t) = \arcsin(\sin i_K \ \sin \alpha_\ell(t)), \tag{3}$$

$$\phi_\ell(t) = \text{mod}\big(\widetilde{\phi}_\ell(t) - \omega_E t + \pi,\ 2\pi\big) - \pi, \tag{4}$$

where ω_E is the Earth's angular velocity, and

$$\widetilde{\phi}_\ell(t) = \text{atan2}(\cos i_K \ \sin \alpha_\ell(t),\ \cos \alpha_\ell(t)), \tag{5}$$

[1]The SSP of satellite ℓ is the point on the Earth's surface lying on the straight line connecting ℓ with the Earth's center.

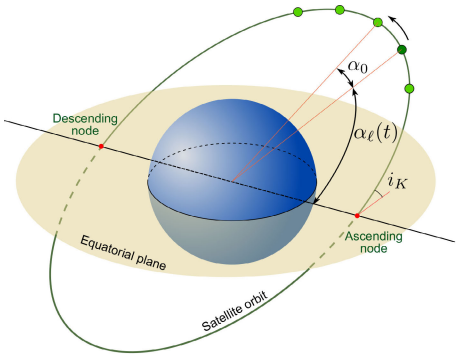

FIGURE 1. N_{Sat} satellites deployed in a circular orbit with inclination i_K relative to the Earth's equatorial plane. Adjacent satellites are evenly spaced with angular separation $\alpha_0 = \frac{2\pi}{N_{\text{Sat}}}$ radians.

with atan2$(\cdot, \cdot)$ denoting the two-argument arctangent function [61].

With reference to Fig. 2, let $(\lambda_{GU}, \phi_{GU})$ denote the latitude and longitude of the GU, assumed fixed during a single satellite pass.[2]

The central angle between the GU and the SSP of satellite ℓ follows from the spherical law of cosines [62], while the elevation angle of satellite ℓ as observed at the GU is derived from the law of sines [60]:

$$\gamma_\ell(t) = \arccos\Big(\sin\lambda_\ell(t)\,\sin\lambda_{GU} + \cos\lambda_\ell(t)\,\cos\lambda_{GU}\,\cos\Delta\phi_\ell(t)\Big),$$

$$\delta_\ell(t) = \arctan\left(\frac{\cos\gamma_\ell(t) - \frac{R_E}{R_E+h_0}}{\sin\gamma_\ell(t)}\right),$$

where $\Delta\phi_\ell(t) = \phi_{GU} - \phi_\ell(t)$.

We define $\delta_{\min}$ as the minimum elevation angle that enables successful communication between the GU and a satellite. Accordingly, the set of visible satellites at time t is

$$\mathcal{V}(t) = \{\ell \in \{1, \ldots, N_{\text{Sat}}\} \mid \delta_\ell(t) \geq \delta_{\min}\}.$$

Among these, the satellite with the highest elevation angle is indexed by $\ell_1(t)$, and the second highest by $\ell_2(t)$. We consider two relaying options: in the first, MSR, the set of relays is defined as the subset $\mathcal{R}(t) = \mathcal{V}(t) \setminus \{\ell_1(t)\}$, while in the second, SSR, $\mathcal{R}(t) = \{\ell_2(t)\}$. For brevity, we often omit the time dependence and write $\mathcal{V}$ and $\mathcal{R}$ instead of $\mathcal{V}(t)$ and $\mathcal{R}(t)$. As illustrated in Fig. 2, the slant distance between satellite $\ell \in \mathcal{V}$ and the GU can be computed using the law of cosines [63]:

$$d_\ell(t) = \sqrt{R_E^2 \sin^2\delta_\ell(t) + h_0^2 + 2\,h_0 R_E} - R_E \sin\delta_\ell(t). \quad (6)$$

Table 1 summarizes the geometrical parameters and variables introduced in this section.

[2]Since a satellite remains in view for only a few minutes, both pedestrian (∼5 km/h) and vehicular (∼50 km/h) mobility can be neglected.

TABLE 1. Constellation geometrical parameters and variables.

Symbol	Definition
N_{Sat}	Constellation size
h_0	Satellite altitude
i_K	Orbit inclination
$\alpha_l(t)$	Angular position of satellite ℓ at time t
$(\lambda_\ell(t), \phi_\ell(t))$	SSP coordinates for satellite ℓ at time t
$(\lambda_{GU}, \phi_{GU})$	GU coordinates
$\gamma_l(t)$	Central angle between GU and SSP of satellite l
$\delta_l(t)$	Elevation of satellite l at time t
$d_l(t)$	Slant distance of satellite l at time t
$\delta_{\min}$	Visible satellite minimum elevation
$\mathcal{V}(t)$	Visible satellite set at time t
$\mathcal{R}(t)$	Relay satellite set at time t

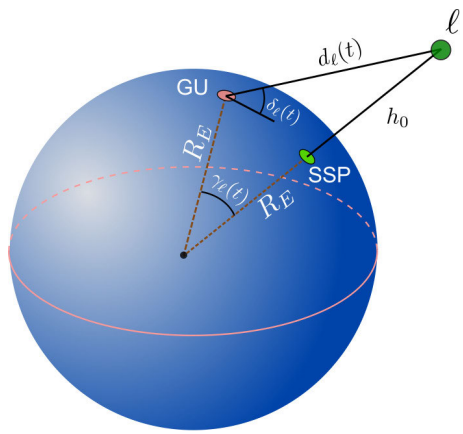

FIGURE 2. Geometric model of satellite ℓ orbiting the Earth at altitude h_0. The satellite elevation angle, as observed by the GU, is denoted by $\delta_\ell(t)$, while $d_\ell(t)$ is the slant distance.

B. CHANNEL MODELS

1) G2S CHANNEL MODEL

For the G2S link, we adopt the narrowband model ITU Recommendation P.681-11 specified in [59] and [63], which is based on a two-state Semi-Markov process with states *good* (G) and *bad* (B). State G represents conditions with low obstruction and mild fading, while state B corresponds to severe shadowing and strong fading. The channel alternates between these states, where the duration of each state is modeled as an independent lognormal random variable with parameters specific to G and B.

Within each state, the small-scale channel coefficients follow the *Loo distribution* [6], which jointly captures lognormal shadowing and Rayleigh multipath fading. This distribution is particularly suitable for G2S channels, as it accounts for both slowly varying attenuation due to terrain or obstacles and fast multipath fluctuations caused by multipath propagation. Compared to classical Rayleigh or Rician models, it provides a more accurate representation of real-world propagation. Each channel coefficient is modeled as a complex random variable with independent magnitude and phase. The phase is uniformly distributed in $[0, 2\pi]$, while the magnitude follows a PDF that incorporates both the direct LoS component and the diffuse multipath component. The

PDF of the coefficient magnitude is given by

$$f_{\text{Loo}}(x) = \frac{8.686\, x}{\Sigma_A \sigma^2 \sqrt{2\pi}} \int_0^{+\infty} \frac{1}{a} \mathrm{e}^{-\frac{(20\log_{10}(a)-M_A)^2}{2\Sigma_A^2} - \frac{x^2-a^2}{2\sigma^2}} \times I_0\left(\frac{ax}{\sigma^2}\right) da \quad (7)$$

where M_A and Σ_A are the mean and standard deviation of the LoS component, respectively, and $I_0(\cdot)$ is the modified Bessel function of the first kind (order 0).

The Loo distribution is fully characterized by the parameter triplet $(M_A, \Sigma_A, \text{MP})$, where $\text{MP} = 10\log_{10}\sigma^2$ denotes the multipath power. These parameters are themselves random variables with state-dependent distributions (G or B) and are sampled independently for each state realization. Temporal correlation across successive channel coefficients is modeled through low-pass filtering of the LoS component and Jakes' spectrum filtering of the scattered component [59].

It is worth noting that, for upper frequency bands such as the V band, new models such as fluctuating two-ray [64] and multi-cluster fluctuating two-ray [65] enable accurate and mathematically simple characterization. However, in this paper, we consider G2S links in the D band, for which the Loo model is better suited.

On the G2S uplink, the instantaneous SNR of the signal received by satellite $\ell \in \mathcal{V}$ at time t is expressed as

$$\text{SNR}_\ell(t) = \frac{P_{GU} G_{GU} G_\ell L_\ell(t) |h_\ell(t)|^2}{N_0 W_{G2S}} = \rho_\ell(t)\, |h_\ell(t)|^2, \quad (8)$$

where

- P_{GU} is the transmit power of the GU;
- G_{GU} and G_ℓ are the antenna gains of the GU and satellite ℓ, respectively;
- $L_\ell(t) = \left(\frac{c}{4\pi d_\ell(t) f_{G2S}}\right)^2$ is the free-space path loss, with c the speed of light and f_{G2S} the G2S carrier frequency;
- $h_\ell(t)$ is the fading and shadowing coefficient of the G2S channel;
- $\rho_\ell(t)$ is the LoS SNR, i.e., the SNR without shadowing or fading;
- N_0 is the noise power spectral density;
- W_{G2S} is the signal bandwidth of the G2S link.

Table 2 summarizes the parameters of the G2S channel model.

TABLE 2. G2S link parameters.

Symbol	Definition
$(M_A, \Sigma_A, \text{MP})$	Loo distribution parameters
P_{GU}	GU transmit power
G_{GU}, G_ℓ	TX and RX antenna gains in ℓ-th G2S link
f_{G2S}	Carrier frequency
N_0	Noise spectral density
W_{G2S}	Signal bandwidth

2) ISL CHANNEL MODEL

For the ISL link, we adopt the model described in [44]. Since ISLs operate at very high frequencies, depolarization effects can be neglected. Similarly, attenuation due to plasma and collision frequencies is negligible compared to the dominant free-space path loss, and is therefore omitted.

Under these assumptions, the ISL reduces to an AWGN channel, where the randomness in the received SNR arises primarily from pointing errors. Such errors are represented by a misalignment angle ξ between the transmit and receive antennas. According to [44], the antenna gain of each satellite is modeled as

$$G = G_0\, \mathrm{e}^{-\nu\xi^2}, \quad (9)$$

where G_0 is the maximum gain (achieved when the antenna boresight is perfectly aligned), and $\nu = 4\ln(2)/\theta_{3dB}^2$ is a constant determined by the 3-dB beamwidth θ_{3dB} of the main lobe.[3] The misalignment angle ξ is modeled as a Gaussian random variable with zero mean and variance σ_p^2.

We focus on ISLs established between the serving satellite (S)—defined as the satellite with the highest elevation as observed by the GU—and all satellites in the set $\mathcal{R}$. Variables related to the serving satellite are denoted by the subscript S (e.g., ρ_S, α_S). The instantaneous received SNR on the ISL between the serving satellite and satellite $\ell \in \mathcal{R}$ is given by

$$\rho_{\text{ISL},\ell} = \frac{P_T L_{\text{ISL},\ell} G_0^2\, \mathrm{e}^{-2\nu\xi^2}}{k_B T_0 W_{\text{ISL}}}, \quad (10)$$

where

- P_T is the ISL transmit power;
- $L_{\text{ISL},\ell} = \left(\frac{c}{4\pi d_{\text{ISL},\ell} f_{\text{ISL}}}\right)^2$ is the free-space path loss, with f_{ISL} the ISL carrier frequency and $d_{\text{ISL},\ell} = 2(R_e + h_0)\sin\left(\frac{\alpha_\ell - \alpha_S}{2}\right)$ the link distance between satellite ℓ and the serving satellite;
- $k_B = 1.38 \times 10^{-23}$ J/K is the Boltzmann constant;
- T_0 is the noise temperature;
- W_{ISL} is the ISL signal bandwidth.

Table 3 summarizes the parameters of the ISL channel model. Throughout this work, unless otherwise stated, we assume perfect receiver knowledge of the ISL SNR.

TABLE 3. ISL parameters.

Symbol	Definition
P_T	Transmit power
G_0	Boresight antenna gain
ν	Antenna misalignment sensitivity
$\theta_{3\text{dB}}$	Antenna 3-dB beamwidth
$\xi \sim \mathcal{N}(0, \sigma_p^2)$	Misalignment angle
f_{ISL}	Carrier frequency
T_0	Noise temperature
W_{ISL}	Bandwidth
$d_{\text{ISL},\ell}$	Link length for relay ℓ
$\rho_{\text{ISL},\ell}$	SNR for relay ℓ

III. SH SCHEME SPECIFICATION

In this section, we specify the proposed SH scheme for LEO satellite constellations. First, we analyze two CSI

[3] We assume circular symmetry of the antenna main lobe.

conditions: an ideal case with perfect CSI and a case with imperfect CSI obtained through pilot-assisted estimation. Second, we investigate two cooperative relaying strategies between the serving and relaying satellites, namely AF and DF. Finally, for both relaying techniques, we derive the received signal after combining at the serving satellite for both MRC and SC.

A. RECEIVED SIGNAL ON THE G2S LINK

The GU encodes its information word $\mathbf{u}$ using a rate-R_c low-density parity-check (LDPC) code, generating a codeword $\mathbf{c}$, which is subsequently modulated into a sequence of unit-energy symbols $\{x[n]\}_{n=1}^{N}$ drawn from a constellation of size S. The n-th symbol is transmitted at time $t_n = nT_s$, where T_s is the symbol period.

The GU broadcasts its signal to the serving satellite S and to all satellites in the relay set $\mathcal{R}$. Each relaying satellite forwards its received signal to the serving satellite through the ISL between them, according to the relaying strategies described in the following section. If, at some instant, a satellite $\ell \in \mathcal{R}$ achieves a higher elevation angle than satellite S (i.e., $\delta_{\mathrm{S}}(t) < \delta_\ell(t)$), their roles are exchanged.

The normalized received signal at satellite $\ell \in \mathcal{V}$ at time step n is

$$y_\ell[n] = \sqrt{\rho_\ell[n]}\, h_\ell[n]\, x[n] + w_\ell[n], \tag{11}$$

where $w_\ell[n] \sim \mathcal{CN}(0,1)$ is circularly symmetric complex Gaussian noise, $\rho_\ell[n] \triangleq \rho_\ell(nT_s)$ is the LoS SNR, and $h_\ell[n] \triangleq h_\ell(nT_s)$ accounts for shadowing and fading. For compactness, we denote $\mathbf{y}_\ell = (y_\ell[1], \ldots, y_\ell[N])$, and similarly for $\boldsymbol{\rho}_\ell$ and $\mathbf{h}_\ell$. For the serving satellite, we use the notation $\mathbf{y}_{\mathrm{S}}$, $\boldsymbol{\rho}_{\mathrm{S}}$ and $\mathbf{h}_{\mathrm{S}}$.

In this work, we analyze two different CSI conditions:

- **Imperfect CSI:** Each satellite estimates its channel using standard maximum-likelihood pilot-assisted technique (see [66, Sect. 3.5.2]). For each satellite $\ell \in \mathcal{V}$ at time n, the estimated channel is given by:

$$\widehat{h}_\ell[n] = h_\ell[n] + w_{\mathrm{CE},\ell}[n], \tag{12}$$

where the estimation error $w_{\mathrm{CE},\ell}[n]$ follows a complex Gaussian distribution:

$$w_{\mathrm{CE},\ell}[n] \sim \mathcal{CN}\left(0, \sigma^2_{\mathrm{CE}}[n]\right),$$

and the error variance is defined as:

$$\sigma^2_{\mathrm{CE}}[n] = \frac{1}{\rho_\ell[n] E_p},$$

with E_p denoting the pilot energy and $\rho_\ell[n]$ the pilot SNR for satellite ℓ at time n.

- **Perfect CSI:** Each satellite is assumed to have exact knowledge of its G2S channel. This idealized scenario corresponds to the limiting case of (12) as the pilot energy $E_p \to \infty$, effectively eliminating estimation errors. Mathematically, for each satellite $\ell \in \mathcal{V}$ at time n, the channel estimate becomes:

$$\widehat{h}_\ell[n] = h_\ell[n] \tag{13}$$

B. SATELLITE RELAYING TECHNIQUES VIA ISL

In the considered SH scenario, satellites in the relay set $\mathcal{R}$ assist the serving satellite S by forwarding the signal received from the GU through ISLs. We explore two cooperative relaying strategies to enable this assistance effectively.

- **AF:** The relay satellite $\ell \in \mathcal{R}$ works as a repeater [67], by simply forwarding its received signal $y_\ell[n]$, after proper power normalization, together with the acquired CSI. The normalized (unit-energy) transmitted signal on the ISL at time step n then becomes

$$x_{\mathrm{AF},\ell}[n] = \frac{y_\ell[n]}{\sqrt{q_\ell[n]}}, \tag{14}$$

where $q_\ell[n]$ is a normalization factor. For perfect CSI, we have

$$q_\ell[n] = \mathbb{E}[|y_\ell[n]|^2] = \rho_\ell[n]|h_\ell[n]|^2 + 1 \tag{15}$$

while for imperfect CSI[4]

$$\begin{aligned} q_\ell[n] &= \rho_\ell[n]\mathbb{E}[|h_\ell[n]|^2] + 1 \\ &= \rho_\ell[n]\mathbb{E}[|\widehat{h}_\ell[n] - w_{\mathrm{CE},\ell}[n]|^2] + 1 \\ &= \rho_\ell[n]\left(|\widehat{h}_\ell[n]|^2 + \sigma^2_{\mathrm{CE}}[n]\right) + 1 \\ &= \rho_\ell[n]|\widehat{h}_\ell[n]|^2 + 1 + \frac{1}{E_p} \end{aligned} \tag{16}$$

The normalized signal in (14) is amplified with an amplification gain prior to transmission.

- **DF:** Each relay satellite $\ell \in \mathcal{R}$ demodulates and decodes its received signal from the GU. A block decoding error may occur with probability P_B, as defined in (IV-A) given below. We assume that the satellite can reliably determine whether the decoding was successful. If decoding is successful, the satellite re-encodes the estimated information bits, modulates the resulting coded bits, and forwards the regenerated signal to the serving satellite S via the ISL, so that:

$$x_{\mathrm{DF},\ell}[n] = x[n], \forall n \tag{17}$$

Otherwise, the satellite remains silent and does not transmit. Notice that with DF, the relay satellite does not need to forward its G2S CSI.

In the general case of imperfect CSI, the normalized signal received by satellite S from relay $\ell \in \mathcal{R}$ will be given by

$$y_{\vartheta,\ell}[n] = \sqrt{\rho_{\mathrm{ISL},\ell}}\, x_{\vartheta,\ell}[n] + w_{\mathrm{ISL},\ell}[n] \tag{18}$$

where $\vartheta \in \{\mathrm{AF}, \mathrm{DF}\}$ and $w_{\mathrm{ISL},\ell}[n] \sim \mathcal{CN}(0,1)$. In the following, we will omit the time index n for brevity.

For AF relays, we have:

$$\begin{aligned} y_{\mathrm{AF},\ell} &= \sqrt{\rho_{\mathrm{ISL},\ell}}\, x_{\mathrm{AF},\ell} + w_{\mathrm{ISL},\ell} \\ &= \sqrt{\frac{\rho_{\mathrm{ISL},\ell}}{q_\ell}}\, y_\ell + w_{\mathrm{ISL},\ell} \end{aligned}$$

[4]Notice that the third equality in (16) only holds if $\widehat{h}_\ell[n]$ and $\sigma^2_{\mathrm{CE}}[n]$ are uncorrelated. Although this is not true, the AF relay behaves as if it were.

$$= \sqrt{\frac{\rho_{\mathrm{ISL},\ell}}{q_\ell}} \left(\sqrt{\rho_\ell} h_\ell x + w_\ell\right) + w_{\mathrm{ISL},\ell}$$
$$= \sqrt{\frac{\rho_{\mathrm{ISL},\ell}}{q_\ell}} \left(\sqrt{\rho_\ell} \left(\widehat{h}_\ell - w_{\mathrm{CE},\ell}\right) x + w_\ell\right) + w_{\mathrm{ISL},\ell}$$
$$= \sigma_{\mathrm{AF},\ell} \left(\left(\widehat{h}_{\mathrm{AF},\ell} - w_{\mathrm{CE,AF},\ell}\right) x + w_{\mathrm{AF},\ell}\right), \quad (19)$$

where $\sigma^2_{\mathrm{AF},\ell} = 1 + \frac{\rho_{\mathrm{ISL},\ell}}{q_\ell}$, $w_{\mathrm{AF},\ell} \sim \mathcal{CN}(0, 1)$, and we defined the estimated instantaneous channel coefficient of the cascade G2S-ISL (through relay ℓ)

$$\widehat{h}_{\mathrm{AF},\ell} = \sqrt{\frac{\rho_{\mathrm{ISL},\ell}\rho_\ell}{q_\ell}} \frac{\widehat{h}_\ell}{\sigma_{\mathrm{AF},\ell}} = \sqrt{\widetilde{\rho}_{\mathrm{AF},\ell}} \widehat{h}_\ell. \quad (20)$$

with the LoS SNR of the cascade being

$$\widetilde{\rho}_{\mathrm{AF},\ell} = \frac{\rho_{\mathrm{ISL},\ell}}{q_\ell + \rho_{\mathrm{ISL},\ell}} \rho_\ell. \quad (21)$$

In (19) we also defined the channel estimation noise

$$w_{\mathrm{CE,AF},\ell} = \sqrt{\widetilde{\rho}_{\mathrm{AF},\ell}} w_{\mathrm{CE},\ell} \sim \mathcal{CN}\left(0, \frac{\widetilde{\rho}_{\mathrm{AF},\ell}}{\rho_\ell E_p}\right). \quad (22)$$

For DF relays, we have in case of successful decoding:

$$y_{\mathrm{DF},\ell} = \sqrt{\rho_{\mathrm{ISL},\ell}} x_{\mathrm{DF},\ell} + w_{\mathrm{ISL},\ell}$$
$$= \sqrt{\rho_{\mathrm{ISL},\ell}} x + w_{\mathrm{ISL},\ell} \quad (23)$$

and we also define $\widehat{h}_{\mathrm{DF},\ell} = \sqrt{\rho_{\mathrm{ISL},\ell}}$, $w_{\mathrm{DF},\ell} = w_{\mathrm{ISL},\ell}$ and $\sigma_{\mathrm{DF},\ell} = 1$.

Finally, the normalized received signal from relay ℓ is given by

$$\widetilde{y}_{\vartheta,\ell} = \frac{y_{\vartheta,\ell}}{\sigma_{\vartheta,\ell}}. \quad (24)$$

for $\vartheta \in \{\mathrm{AF}, \mathrm{DF}\}$.

C. PROCESSING AT THE SERVING SATELLITE

Satellite S receives both the direct G2S signal from the GU and the relayed ISL signals from all satellites in the relay set $\mathcal{R}$. We will develop the equations for the imperfect CSI case, since it is the more general. The case of perfect CSI can be obtained in the limit $E_p \to \infty$. To exploit spatial diversity, satellite S combines the direct G2S signal with the relayed ISL signals. For DF relays, let us define $\mathcal{R}_{\mathrm{DF}} \subseteq \mathcal{R}$ as the subset of relays that successfully decode their received signals and thus forward them to satellite S. For convenience, we also define $\mathcal{R}_{\mathrm{AF}} = \mathcal{R}$. We explore two different combining techniques.

- MRC: all received signals are combined with weights proportional to their qualities, so that MRC achieves both diversity and array gains. The output of the MRC combiner is given by

$$y_{\mathrm{MRC},\vartheta} = \sqrt{\rho_{\mathrm{S}}} \widehat{h}^*_{\mathrm{S}} y_{\mathrm{S}} + \sum_{\ell \in \mathcal{R}_\vartheta} \widehat{h}^*_{\vartheta,\ell} \widetilde{y}_{\vartheta,\ell}$$
$$= \left(\rho_{\mathrm{S}} |\widehat{h}_{\mathrm{S}}|^2 + \sum_{\ell \in \mathcal{R}_\vartheta} |\widehat{h}_{\vartheta,\ell}|^2\right) x$$
$$- \left(\rho_{\mathrm{S}} \widehat{h}^*_{\mathrm{S}} w_{\mathrm{CE,S}} + \sum_{\ell \in \mathcal{R}_\vartheta} \widehat{h}^*_{\vartheta,\ell} w_{\mathrm{CE},\vartheta,\ell}\right) x$$
$$+ \left(\sqrt{\rho_{\mathrm{S}}} \widehat{h}^*_{\mathrm{S}} w_{\mathrm{S}} + \sum_{\ell \in \mathcal{R}_\vartheta} \widehat{h}^*_{\vartheta,\ell} w_{\vartheta,\ell}\right)$$
$$= \left(\rho_{\mathrm{MRC},\vartheta} - w_{\mathrm{CE,MRC},\vartheta}\right) x + \sqrt{\rho_{\mathrm{MRC},\vartheta}} w_{\mathrm{MRC},\vartheta} \quad (25)$$

  where:

$$\rho_{\mathrm{MRC},\vartheta} = \rho_{\mathrm{S}} |\widehat{h}_{\mathrm{S}}|^2 + \sum_{\ell \in \mathcal{R}_\vartheta} |\widehat{h}_{\vartheta,\ell}|^2,$$
$$w_{\mathrm{MRC},\vartheta} \sim \mathcal{CN}(0, 1)$$

  for $\vartheta \in \{\mathrm{AF}, \mathrm{DF}\}$. Moreover,

$$w_{\mathrm{CE,MRC,AF}} \sim \mathcal{CN}\left(0, \frac{\rho_{\mathrm{S}} |\widehat{h}_{\mathrm{S}}|^2}{E_p} + \sum_{\ell \in \mathcal{R}} \frac{\widetilde{\rho}^2_{\mathrm{AF},\ell}}{\rho_\ell} \frac{|\widehat{h}_\ell|^2}{E_p}\right)$$
$$w_{\mathrm{CE,MRC,DF}} \sim \mathcal{CN}\left(0, \frac{\rho_{\mathrm{S}} |\widehat{h}_{\mathrm{S}}|^2}{E_p}\right)$$

  Finally, we define the normalized MRC output as:

$$\widetilde{y}_{\mathrm{MRC},\vartheta} = \frac{y_{\mathrm{MRC},\vartheta}}{\sqrt{\rho_{\mathrm{MRC},\vartheta}}}. \quad (26)$$

- SC: SC is a low-complexity diversity technique in which the receiver selects the branch with the highest instantaneous SNR and discards the others. This method provides diversity gain without requiring phase synchronization across branches. Satellite S selects the signal with the maximum instantaneous SNR among those received from the GU and from the relays. Let

$$\ell^* = \arg\max_{\ell \in \mathcal{R}_\vartheta} |\widehat{h}_{\vartheta,\ell}|, \quad \vartheta \in \{\mathrm{AF}, \mathrm{DF}\}$$

  be the index of the relay satellite with the largest instantaneous SNR. Then:

$$\widetilde{y}_{\mathrm{SC},\vartheta} = \begin{cases} y_S, & \text{if } \rho_{\mathrm{S}} |\widehat{h}_{\mathrm{S}}|^2 \geq |\widehat{h}_{\vartheta,\ell^*}|^2, \\ \widetilde{y}_{\vartheta,\ell^*}, & \text{if } \rho_{\mathrm{S}} |\widehat{h}_{\mathrm{S}}|^2 < |\widehat{h}_{\vartheta,\ell^*}|^2, \end{cases} \quad (27)$$

  for $\vartheta \in \{\mathrm{AF}, \mathrm{DF}\}$. The corresponding instantaneous SNR is $\rho_{\mathrm{SC},\vartheta} = \max\left\{\rho_{\mathrm{S}} |\widehat{h}_{\mathrm{S}}|^2, |\widehat{h}_{\vartheta,\ell^*}|^2\right\}$.

This completes the specification of the SH scheme under imperfect CSI, with AF and DF relaying strategies, and with MRC or SC combining techniques. Table 4 summarizes the parameters and variables that describe the communication system.

IV. PERFORMANCE ANALYSIS

In this section, we define the BLER as the main performance parameter and we analyze the proposed SH-MSR system from that point of view. In particular, we first give an information-theoretic definition of BLER, which forms the basis on which it is computed in Section V. Then, we provide theoretical insights on the BLER performance in some particular corner cases.

TABLE 4. Communication system parameters and variables.

Symbol	Definition
R_c	Channel coding rate
N_c	Codeword length in symbols
C_T	Channel decoding threshold
S	Modulation size
E_P	Pilot energy
σ^2_{CE}	Variance of the channel estimation error
$x[n]$	Transmitted symbol in step n
$y_\ell[n]$	Received sample at relay ℓ in step n
$\rho_\ell[n], h_\ell[n]$	LoS SNR and channel coefficient for relay ℓ in step n
$\rho_S[n], h_S[n]$	LoS SNR and channel coefficient for satellite S in step n
$\widehat{h}_\ell[n], \widehat{h}_S[n]$	Estimates of $h_\ell[n]$ and $h_S[n]$
$q_\ell[n] = E[\lvert y_l[n]\rvert^2]$	Power of received signal at relay ℓ in step n
$x_{\theta,\ell}[n]$	Signal forwarded by relay ℓ in step n ($\theta \in \{\mathrm{AF}, \mathrm{DF}\}$)
$y_{\theta,\ell}[n]$	Signal received from relay ℓ in step n ($\theta \in \{\mathrm{AF}, \mathrm{DF}\}$)
$\widehat{h}_{\theta,\ell}[n]$	Estimated channel coefficient from relay ℓ in step n
$\sigma^2_{\theta,\ell}[n]$	Variance of noise sample in $y_{\theta,\ell}[n]$
$\widetilde{y}_{\theta,\ell}[n]$	Normalized version of $y_{\theta,\ell}[n]$
$\widehat{\rho}_{\mathrm{AF},\ell}[n]$	Estimated SNR of the cascade G2S-ISL for AF relaying
$\widetilde{y}_{\eta,\vartheta}[n]$	Normalized combiner output ($\eta \in \{\mathrm{MRC}, \mathrm{SC}\}$, $\theta \in \{\mathrm{AF}, \mathrm{DF}\}$)
$\rho_{\eta,\vartheta}[n]$	Estimated combiner output SNR

A. INFORMATION-THEORETIC BLER FRAMEWORK

We consider the BLER after combining at satellite S as the performance parameter of the considered SH scheme. In doing this, we suppose that the belief-propagation (BP) decoder of the LDPC code works as a threshold device, namely it succeeds in decoding if and only if the input mutual information (MI) per received bit exceeds a given code-dependent threshold C_T. This is a good approximation of the real BP decoder behavior when the block length is large enough [68], which is the case of interest in NTN communications.

Consider the AWGN channel $\mathcal{Y} = \sqrt{\rho}\mathcal{H}\mathcal{X} + \mathcal{W}$, where $\mathcal{W} \sim \mathcal{CN}(0, 1)$, $\mathcal{H}$ is unknown and distributed according to pdf $f_{\mathcal{H}}$ and $\mathcal{X}$ is uniform on a size-S modulation $\mathcal{S}$. The receiver knows a noisy version of $\mathcal{H}$, denoted $\widehat{\mathcal{H}} = \mathcal{H} + \mathcal{W}_{CE}$, $\mathcal{W}_{CE} \sim \mathcal{CN}(0, \sigma^2_{CE})$ being the channel estimation error. In the following, we compute the average MI on this channel, under some simplifying assumptions. Let $H\left(\mathcal{X}|y, \rho, \widehat{h}\right)$ be the equivocation on such channel when $\mathcal{Y}$=y
and $\widehat{\mathcal{H}}$=$\widehat{h}$, i.e.,

$$H\left(\mathcal{X}|y, \rho, \widehat{h}\right) = -\sum_{s\in\mathcal{S}} p\left(s|y, \rho, \widehat{h}\right) \log_2 p\left(s|y, \rho, \widehat{h}\right) \quad (28)$$

where $p\left(s|y, \rho, \widehat{h}\right)$ is the a-posteriori probability of the event $\{\mathcal{X} = s\}$ given the received sample and the estimated channel coefficient. To compute it, let us first derive the distribution of $\mathcal{W}_{CE}$ conditional on $\widehat{\mathcal{H}} = \widehat{h}$. We have

$$f_{\mathcal{W}_{CE}|\widehat{\mathcal{H}}}(w|\widehat{h}) = \frac{f_{\mathcal{H}}(\widehat{h} - w)\mathrm{e}^{-|w|^2/\sigma^2_{CE}}}{\int f_{\mathcal{H}}(\widehat{h} - w')\mathrm{e}^{-|w'|^2/\sigma^2_{CE}}\, dw'} \quad (29)$$

In the following, we will suppose that $f_{\mathcal{H}}(\widehat{h} - w)$ can be approximated as uniform for values of w for which the numerator of (29) is non-negligible. This is tantamount to say that $\mathcal{W}_{CE}$ can be considered approximately independent of $\widehat{\mathcal{H}}$, a hypothesis that holds true for a moderate value of σ^2_{CE}. With this approximation, we can write

$$p\left(s|y, \rho, \widehat{h}\right) = K\exp\left\{-\frac{|y - \sqrt{\rho}\widehat{h}s|^2}{\rho|s|^2\sigma^2_{CE} + 1}\right\} \quad (30)$$

where K is a normalization constant. Then, the (conditional) mutual information (MI) per bit is given by

$$C(y, \rho, \widehat{h}) = 1 - \frac{1}{\log_2 S} H\left(\mathcal{X}|y, \rho, \widehat{h}\right) \quad (31)$$

Using a channel code of length N_c symbols to transmit on the considered channel, we model the BLER of the corresponding channel decoder as

$$P_B(e|\mathbf{y}, \boldsymbol{\rho}, \widehat{\mathbf{h}}) = I_{\{\overline{C}(\mathbf{y}, \boldsymbol{\rho}, \widehat{\mathbf{h}}) \le C_T\}} \quad (32)$$

where $\mathbf{y}, \widehat{\mathbf{h}}, \boldsymbol{\rho}$ denote the length-N_c vectors of the received samples $y[n]$, estimated channel coefficients $\widehat{h}[n]$, and SNR values $\rho[n]$, respectively and

$$\overline{C}(\mathbf{y}, \boldsymbol{\rho}, \widehat{\mathbf{h}}) = \frac{1}{N_c}\sum_{n=1}^{N_c} C(y[n], \rho[n], \widehat{h}[n]) \quad (33)$$

is the average MI per bit on the code block.

Let us define $\widetilde{h}_{\eta,\vartheta}[n] = \sqrt{\rho_{\eta,\vartheta}[n]}$, $\eta \in \{\mathrm{MRC}, \mathrm{SC}\}$, $\vartheta \in \{\mathrm{AF}, \mathrm{DF}\}$. With reference to (26), (25) for MRC and (27) for SC, the performance in terms of BLER of the SH scheme will be given by

$$P_{B,\mathrm{SH},\eta,\vartheta}(e) = \mathbb{E}_{\widetilde{\mathbf{y}}_{\eta,\vartheta}, \widetilde{\mathbf{h}}_{\eta,\vartheta}} P_B(e|\widetilde{\mathbf{y}}_{\eta,\vartheta}, \mathbf{1}, \widetilde{\mathbf{h}}_{\eta,\vartheta}) \quad (34)$$

where $\eta \in \{\mathrm{MRC}, \mathrm{SC}\}$, $\vartheta \in \{\mathrm{AF}, \mathrm{DF}\}$, $\mathbb{E}_z$ is the average with respect to random variable z and $\mathbf{1}$ is an all-1 vector.

As a comparison, the BLER performance for the HH method, where the GU is received only by the serving

satellite, without any multi-satellite reception, is

$$P_{B,\mathrm{HH}}(e) = \mathbb{E}_{\widehat{\mathbf{y}}_\mathrm{S},\widehat{\mathbf{h}}_\mathrm{S},\boldsymbol{\rho}_\mathrm{S}} P_B(e|\widehat{\mathbf{y}}_\mathrm{S}, \boldsymbol{\rho}_\mathrm{S}, \widehat{\mathbf{h}}_\mathrm{S}). \tag{35}$$

All the above analysis holds for the imperfect CSI scenario. The case of perfect CSI can be obtained by simply setting $\sigma_{CE}^2 = 0$ in (30). Everything else remains the same.

B. ANALYTICAL RESULTS

In this subsection, we derive some analytical results regarding the BLER of the different variants of the system introduced in the previous sections. First of all, the following proposition, reveals that, even in the presence of imperfect CSI, no matter what the channel realization is, MRC has a better average performance than SC, provided that pilots are transmitted with a suitable power.

Proposition 1: Under the approximation of low channel-estimation noise for which (30) holds, if the pilot power satisfies $E_p \geq \max_{s\in\mathcal{S}} |s|^2$, we have

$$P_{B,\mathrm{SH,MRC},\vartheta}(e) < P_{B,\mathrm{SH,SC},\vartheta}(e) \tag{36}$$

for $\vartheta \in \{\mathrm{AF}, \mathrm{DF}\}$.

Proof: In the appendix, we actually prove a stronger statement, i.e., that, given $\widetilde{\mathbf{h}}_{\eta,\vartheta}[n]$, the instantaneous SNR of $\widetilde{y}_{\mathrm{MRC},\ell}[n]$ in (26) is larger than the instantaneous SNR of $\widetilde{y}_{\mathrm{SC},\vartheta}[n]$ in (27) for $E_p \geq \max_{s\in\mathcal{S}} |s|^2$. Due to the monotonicity of (31) with respect to $\sqrt{\rho}\widehat{h}$ when $\rho\sigma_{CE}^2 = \frac{1}{E_p}$, this implies (36). ■

Although MRC performs better than SC, it entails a larger computational complexity. In some conditions where one of the branches is significantly stronger than the others (e.g., when one of the satellites is momentarily in LoS with respect to the GU), SC could be the best trade-off between performance and complexity.

Now, we consider the performance of AF for $\rho_\mathrm{ISL} \to \infty$. Let $\overline{\mathrm{SNR}}_{\eta,\mathrm{AF}}[n] = \lim_{\rho_\mathrm{ISL}\to\infty} \lim_{E_p\to\infty} \mathrm{SNR}_{\eta,AF}[n]$, for $\eta \in \{\mathrm{MRC}, \mathrm{SC}\}$, be the SNR with perfect CSI and ideal ISL. With a simple application of Jensen's inequality [69], we can bound the asymptotic penalty due to imperfect CSI on the SNR of AF as follows:

$$\frac{\min_{s\in\mathcal{S}} |s|^2}{1+1/E_p} \leq \frac{\lim_{\rho_\mathrm{ISL}\to\infty} \mathrm{SNR}_{\eta,\mathrm{AF}}[n]}{\overline{\mathrm{SNR}}_{\eta,\mathrm{AF}}[n]} \leq \frac{1}{1+1/E_p} \tag{37}$$

for $\eta \in \{\mathrm{MRC}, \mathrm{SC}\}$. Notice that both bounds are tight when $\min_{s\in\mathcal{S}} |s|^2 = 1$, like in PSK constellations.

For perfect CSI ($E_p \to \infty$) and perfect ISL ($\rho_\mathrm{ISL} \to \infty$), AF can be shown to be better than DF. In such a case, indeed, the considered system is equivalent to a virtual $1 \times (|\mathcal{R}| + 1)$ single-input multiple-output system, in which there is only one satellite with $|\mathcal{R}| + 1$ antennas, and the received signal is $\left(\mathbf{y}_\mathrm{S}, \{\mathbf{y}_\ell\}_{\ell\in\mathcal{R}}\right)$. Notice that, given the LoS SNRs of the satellites, the different branches are independent. Thus, the optimal receiver performs MRC *before decoding*, as in the AF case. In such a scenario, the DF strategy corresponds to separate decoding of the branches, so that the transmitted block is lost if and only if all decoding attempts fail, i.e.

$$\lim_{\rho_\mathrm{ISL}\to\infty} P_{B,\mathrm{SH,DF}}(e) = \mathbb{E}_{\boldsymbol{\rho}_\mathrm{S},\boldsymbol{\rho}_\ell}\Bigg\{\mathbb{E}_{\mathbf{y}_\mathrm{S},\mathbf{h}_\mathrm{S}} P_B(e|\mathbf{y}_\mathrm{S}, \boldsymbol{\rho}_\mathrm{S}, \mathbf{h}_\mathrm{S}) \times \prod_{\ell\in\mathcal{R}_\mathrm{DF}} \mathbb{E}_{\mathbf{y}_\ell,\mathbf{h}_\ell} P_B(e|\mathbf{y}_\ell, \boldsymbol{\rho}_\ell, \mathbf{h}_\ell)\Bigg\}. \tag{38}$$

V. SIMULATION RESULTS

In this section, we present the simulation results of our model for satellite uplink under MSR and SSR scenarios. We remind that, when the MSR reception case is considered, the satellite with the highest elevation angle, designated as the serving satellite, receives the GU's signal both directly and by relaying from the other visible satellites. Instead, with SSR reception, the serving satellite processes only the signal from the GU and the one forwarded by the second highest satellite. The latter approach limits reception diversity but can potentially reduce system complexity.

In Table 5, we summarize the default parameters used in the simulations, unless otherwise specified. We study a satellite constellation in one orbital pass, starting from the moment that a given satellite first reaches an elevation angle equal to δ_min, until it becomes no longer visible to the GU, that is, when its elevation angle drops below δ_min. The elevation angle time series of the satellites is quantized to the set $\{20°, 30°, 45°, 60°, 70°\}$, for which corresponding channel parameter tables are provided in [59, Annex 2,Sec. 2.2]. Based on these parameters, the channel coefficients for each G2S link are generated independently. The visibility duration of a single satellite ranges from approximately 2 to 8 minutes, depending on the minimum elevation angle. The codeword duration is assumed to be 0.4 s.

TABLE 5. Simulation parameters.

Parameter	Value	Parameter	Value
Geometrical model		Transmitted signal format	
h_0	550 km	R_c	1/2
i_K	45°	LDPC code	Regular (3, 6)
N_Sat	See text	C_T	0.507 bits
$(\lambda_{GU}, \phi_{GU})$	(45° N, 7° E)	S	4
δ_min	37.5°	Modulation	QPSK
Ground-to-satellite link		Inter-satellite link	
f_G2S	2.2 GHz	f_ISL	193 THz
P_{GU}	10 Watt	P_T	20 dBW
G_{GU}	0 dBi	T_0	7000 K
$G_\ell,\ \ell \in \mathcal{V}$	50 dBi	W_ISL	2% f_{ISL}
W_{G2S}	5 MHz	G_0	90 dBi
Environment	Suburban	θ_{3dB}	0.0064 deg
N_0	-174 dBm/Hz	σ_p^2	See text

In the simulations, we consider as the independent variable a reference SNR, which is the LoS SNR when the satellite is at the minimum distance (i.e., the maximum elevation) from the GU. In other words, the reference SNR for satellite ℓ is

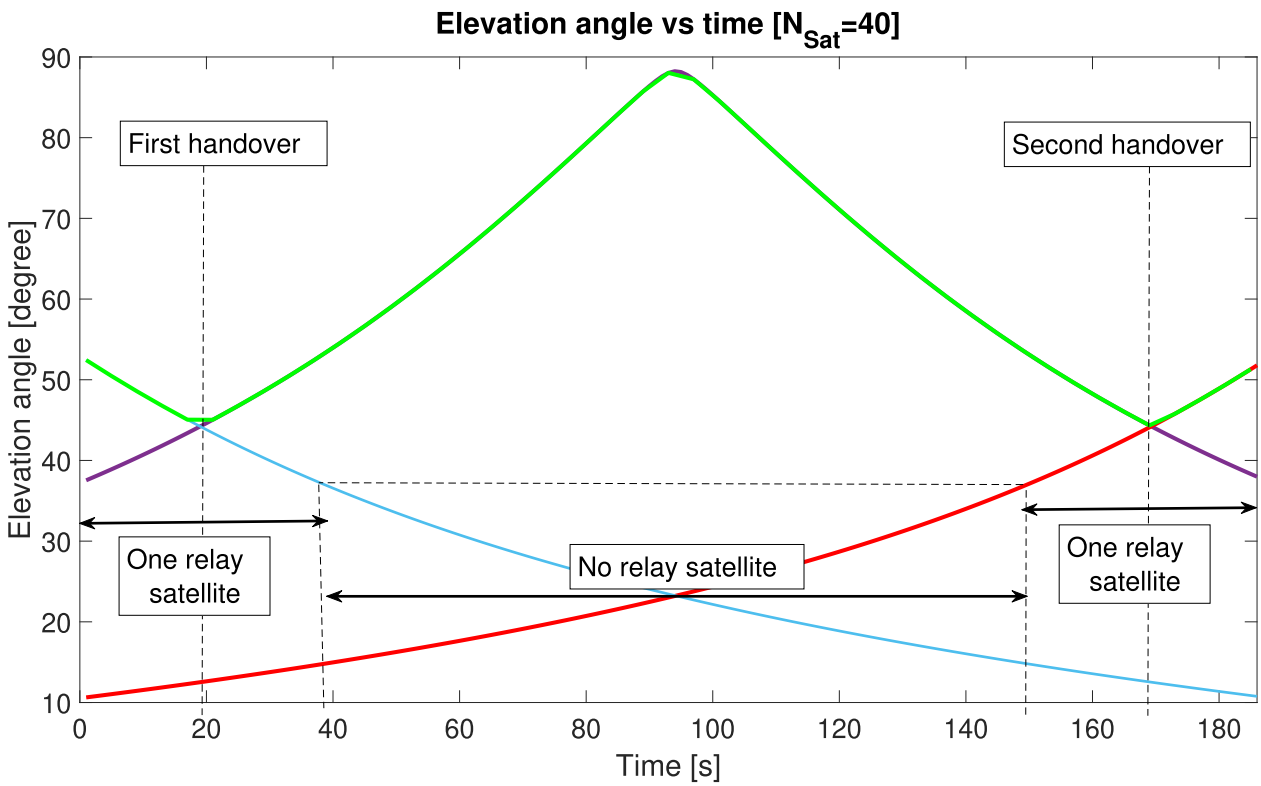

FIGURE 3. Satellite elevation angles during one serving satellite passage. $\delta_{\min} = 37.5°$.

given by

$$\rho_{\text{ref}} = \frac{P_{GU} G_{GU} G_{\ell} L_{\text{ref}}}{N_0 W_{G2S}} \tag{39}$$

where

$$L_{\text{ref}} = \left(\frac{c}{4\pi h_0 f_{G2S}} \right)^2 \tag{40}$$

so that the actual LoS SNR is $\rho_{\ell}[n] = \rho_{\text{ref}} \frac{L_{\ell}[n]}{L_{\text{ref}}}$. The GU transmit power can be derived from the reference SNR. For instance, with the parameters reported in Table 5, a reference SNR of 20 dB corresponds to a transmitted power P_{GU} of about 50 mW.

Unless otherwise stated, all the following subsections assume perfect CSI, an ISL with no misalignment operating at $f_{\text{ISL}} = 193$ THz, a minimum elevation angle of $\delta_{\min} = 37.5°$, a BLER target of 10^{-4}, a satellite transmit power of $P_{\text{T}} = 20$ dBW on the ISL, and the use of MRC as the combining technique.

A. IMPACT OF MINIMUM ELEVATION ANGLE

Figure 3 illustrates the real and quantized elevation angles of a 40-satellite system over one orbital pass as functions of time, together with the corresponding handover procedures for a minimum elevation angle of $\delta_{\min} = 37.5°$. Within the considered time window, two handovers occur. The first takes place at $t = 19$ s, when the purple satellite becomes the closest to the GU and transitions from a relay satellite to the serving satellite. Simultaneously, the blue satellite, previously serving the GU, is reassigned as a relay satellite. At $t = 38$ s, the quantized elevation angle of the blue satellite drops below $\delta_{\min}$, indicating that it is no more visible from the GU. From this point, the system operates with no relaying satellites until $t = 152$ s, when the red satellite becomes visible and starts receiving signals from the GU, thus acting as a new relay satellite. After 20 seconds, at $t = 170$ s, the second handover occurs: the red satellite becomes the new serving satellite, while the purple satellite takes the role of relay and eventually loses its connection with the GU permanently after 20 s.

Table 6 summarizes the impact of $\delta_{\min}$ on the duration of a single satellite pass (i.e., the time a satellite remains above $\delta_{\min}$). As expected, the visibility period is inversely proportional to $\delta_{\min}$, since lower values of $\delta_{\min}$ allow satellites to receive the GU uplink signal even at lower elevation angles. Table 6 also reports the number of available relay satellites and their corresponding time-availability fractions, for different constellation sizes N_{Sat}. For example, with $N_{\text{Sat}} = 100$, the system provides approximately four available relays ($|\mathcal{R}| = 4$) for one-third of the time when $\delta_{\min} = 25°$, whereas this number increases to eight ($|\mathcal{R}| = 8$) when $\delta_{\min} = 10°$, offering a greater diversity of relay options

TABLE 6. Passage duration, serving time, and probability of establishing one or multiple relay connections as a function of satellite constellation size and minimum elevation angle.

Minimum Elevation Angle $\delta_{\min}$	Passage Duration [s]	Number of Satellites N_{Sat}	Serving time [s]	Number of relays (and time fraction)
37,5	186	40	150	1 Sat (38,7%) or 0 Sat, (61,3%)
		60	100	1 Sat (92,5%) or 0 Sat (7,5%)
		80	75	2 Sat (58%) or 1 Sat (42%)
		100	60	3 Sat (13,5%) or 2 Sat (86,5%)
25	282	40	150	1 Sat (93,6%) or 0 Sat, (6,4%)
		60	100	2 Sat (86,8%) or 1 Sat, (13,2%)
		80	75	3 Sat (80%) or 2 Sat, (20%)
		100	60	4 Sat (34%) or 3 Sat, (66%)
10	499	40	150	3 Sat (61%) or 2 Sat, (39%)
		60	100	4 Sat (99%) or 3 Sat, (1%)
		80	75	6 Sat (68,5%) or 5 Sat, (31,5%)
		100	60	8 Sat (34%) or 7 Sat, (66%)

for the serving satellite. Furthermore, denser constellations influence the handover rate. In the 40-satellite configuration, each serving satellite maintains its link for about 150 s, resulting in less frequent handovers. In contrast, for the 100-satellite constellation, the average handover interval decreases to approximately 60 s, indicating that higher satellite density leads to more frequent handover events.

Figure 4 illustrates the impact of $\delta_{\min}$ on the system performance, showing the BLER as a function of the G2S reference SNR under AF relaying technique. A higher elevation threshold reduces the number of satellites eligible to assist the GU, thereby limiting the achievable spatial diversity. In the SSR case, this degradation is less pronounced, since the relay satellite is always selected as the second highest, and reducing $\delta_{\min}$ only slightly decreases its visibility period. In contrast, the MSR configuration benefits substantially from a lower elevation threshold. Decreasing $\delta_{\min}$ (e.g., from 37.5° to 10°) allows a larger set of relay satellites (e.g., from 3 relays to 8 relays for $\delta_{min} = 10$), thereby improving link reliability and reducing the required SNR to achieve a given BLER target. For instance, for a BLER of 10^{-4} and $\delta_{\min} = 10°$, a gain of approximately 7 dB is observed compared to the SSR case. Even in the worst-case scenario—corresponding to the highest $\delta_{\min}$—the MSR configuration still achieves about a 3 dB improvement over the SSR. Furthermore, when comparing MSR to the HH benchmark for $\delta_{\min} = 10°$, the proposed system achieves up to 16 dB gain, highlighting its robustness and efficiency.

In the subsequent simulation analyses, we fix $\delta_{\min} = 37.5°$ to emphasize the gain of SSR/MSR even with a tighter constraint on visibility.

B. CONSTELLATION SIZE

Figure 5 illustrates the reference G2S SNR needed to achieve a given target BLER, as a function of the satellite constellation size N_{Sat}, under different target BLER values, for the conventional HH scheme and the proposed SH-MSR, evaluated with both AF and DF relaying techniques. For a target BLER of 10^{-4}, the HH scheme exhibits only marginal improvements with increasing constellation size, with a reduction of the reference SNR by merely 2 dB

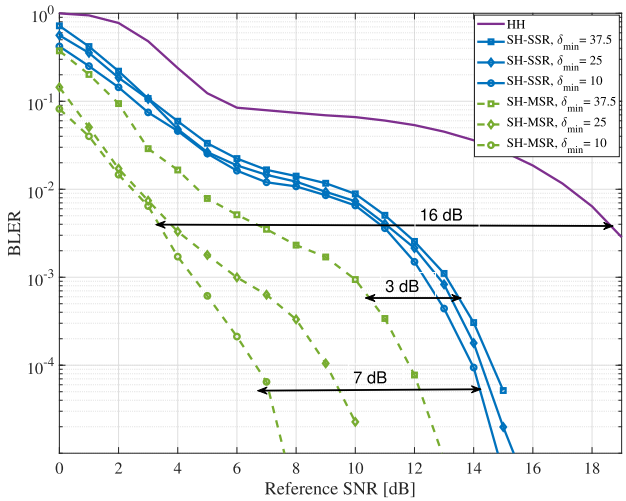

FIGURE 4. Impact of the minimum elevation angle $\delta_{\min}$ on the BLER with HH, SH-SSR, SH-MSR for $N_{\text{Sat}} = 100$, and AF - MRC.

when going from $N_{\text{Sat}} = 40$ to $N_{\text{Sat}} = 100$, and no performance gain beyond $N_{\text{Sat}} \approx 60$. In contrast, SH-MSR yields a significantly larger gain: in the same range, MSR with DF achieves a reduction in reference SNR of nearly 5 dB, while MSR with AF attains up to 10 dB—approximately five times the improvement obtained with HH. These results clearly demonstrate that SH-MSR scales far more effectively with constellation size, offering substantial performance advantages over the conventional HH system, reflecting the diversity gain achieved by the proposed multi-relay scheme.

Another noteworthy observation is that, for both moderate (10^{-3}) and stringent (10^{-4}) BLER targets, AF and DF perform similarly up to a constellation size of about 60 satellites. Beyond this point, AF consistently outperforms DF. This is because DF relays can forward the GU signal only if the received mutual information exceeds a certain threshold, which occurs infrequently; as a result, the relay satellite often fails to transmit the required signal to the serving satellite. In contrast, AF relays do not require decoding and can directly retransmit the received signal, ensuring more reliable delivery. For instance, with

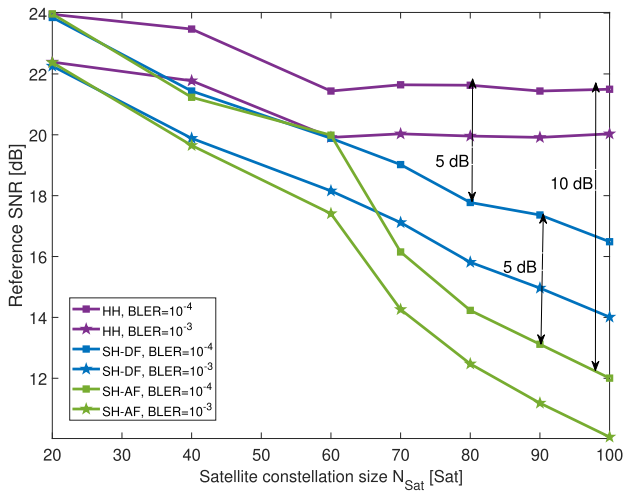

FIGURE 5. Reference SNR required in the G2S link as a function of satellite constellation size N_{Sat}, for different target BLER constraints and relaying techniques, under MRC.

$N_{\text{Sat}} = 100$, SH-AF provides roughly a 5 dB advantage—the same margin maintained for dense constellations with more than 75 satellites. This consistent gain underscores the robustness of AF relaying in exploiting larger constellations, achieving significant performance improvements without additional transmit power or user-side complexity. Since AF relaying consistently outperforms DF in the considered scenarios, AF will be adopted as the relaying scheme throughout the remainder of this work.

C. MISALIGNMENT EFFECT

In this subsection, we evaluate the impact of ISL misalignment on the G2S reference SNR required to achieve a target BLER of 10^{-4}. Fig. 6 presents the performance of SSR and MSR for $N_{\text{Sat}} = 100$, with two ISL scenarios: an optical ISL at $f_{\text{ISL}} = 193$ THz with antenna gain of 90 dBi, and an ISL at $f_{\text{ISL}} = 2$ THz with antenna gain of 50 dBi. We consider two ISL CSI assumptions: *perfect estimation* (solid lines in Fig. 6), where the instantaneous pointing loss is known, and *imperfect estimation* (dashed lines), where the receiver assumes only free-space path loss and ignores instantaneous misalignment.

Under ideal alignment conditions ($\sigma_p \lesssim 10^{-9}$), SH-MSR achieves an SNR gain of approximately 3 dB over SH-SSR. However, as σ_p increases, the performance gap between MSR and SSR rapidly diminishes. For the optical ISL, beyond $\sigma_p \approx 5 \times 10^{-8}$, both MSR and SSR converge to the HH performance, indicating that misalignment prevents effective relaying and nullifies the benefits of cooperative reception. The optical ISL at 193 THz is particularly sensitive to misalignment due to the very narrow beamwidth, such that even small angular deviations result in severe SNR losses.

In the case of imperfect CSI estimation, the receiver ignores the misalignment loss and overestimates the ISL quality, which leads to mismatched MRC weights and to a degradation of the BLER performance. As observed in Fig. 6, this effect is more pronounced in MSR than in SSR, with an SNR penalty of approximately 6.2 dB for SSR and up to 7.8 dB for MSR, since the mismatch accumulates across multiple relays. In contrast, for the 2-THz ISL, due to the much larger beamwidth, the ISL quality is intrinsically robust to pointing errors, and performance degradation becomes noticeable only beyond $\sigma_p \approx 5 \times 10^{-6}$. This significantly higher tolerance to misalignment (up to 2000 times compared to the optical case), explains also why perfect and imperfect estimation yield nearly identical performance for $f_{\text{ISL}} = 2$ THz.

Overall, these results highlight a fundamental trade-off between performance and robustness. While optical ISLs enable higher peak gains under accurate alignment and estimation, they are highly sensitive to misalignment. On the other hand, 2-THz ISLs provide lower peak performance but exhibit strong robustness to pointing errors, making them attractive for practical deployments with relaxed alignment constraints. Nevertheless, from a system-level perspective, optical ISLs remain preferable due to their significantly larger available bandwidth, which can provide roughly two orders of magnitude higher capacity under comparable assumptions. For this reason, the optical ISL configuration is considered in the remainder of this work.

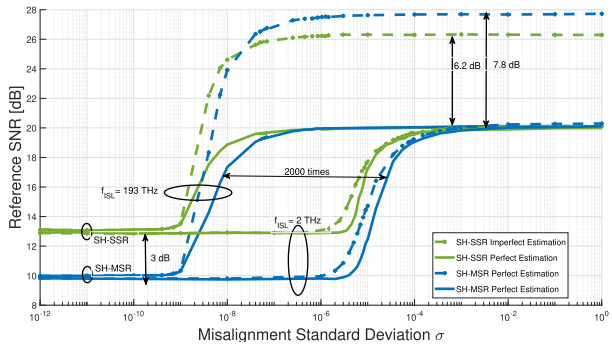

FIGURE 6. Effect of ISL misalignment on SH-MSR and SH-SSR reception, for $f_{\text{ISL}} = 193$ THz and $f_{\text{ISL}} = 2$ THz, under MRC.

D. IMPACT OF RELAY TRANSMIT POWER

This subsection investigates how the relay transmit power P_T influences the G2S reference SNR required to achieve a target BLER of 10^{-4}. Figure 7 presents the corresponding results for constellations of 40 and 100 satellites, illustrating the interplay between relay power, constellation density, and reception technique.

For $N_{\text{Sat}} = 40$, the performance of SH with SSR and MSR reception is identical, since only one relay satellite can actively participate in forwarding, effectively making the two schemes equivalent. Nevertheless, SH still delivers a clear improvement over the conventional HH scenario: the required G2S reference SNR is about 2 dB lower with SH. Remarkably, SH with 40 satellites achieves nearly the same performance as HH with a 100-satellite constellation, implying that cooperative relaying can reduce the constellation size by roughly 60% while preserving the

same reliability. This result highlights the potential of SH to translate spatial cooperation directly into constellation cost savings.

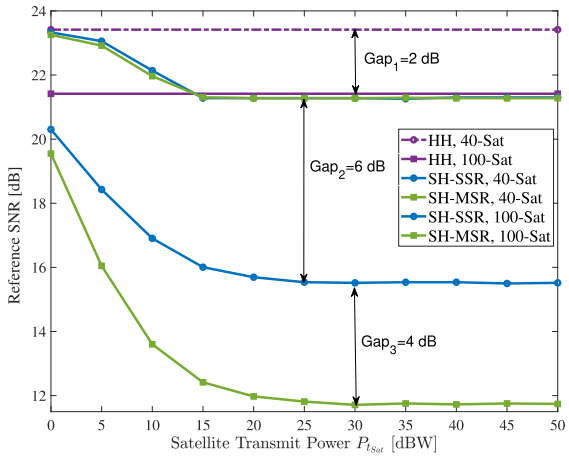

FIGURE 7. G2S reference SNR required to achieve a BLER of 10^{-4} versus relay transmit power P_T under MRC.

When the constellation size increases to $N_{\text{Sat}} = 100$, the advantages of SH become even more pronounced. At $P_T = 20$ dBW, MSR achieves approximately 4-dB gain over SSR and nearly 10-dB gain over HH. Notably, even SSR alone provides a 6 dB improvement compared to HH and the 40-satellite constellation scenario. Beyond $P_T = 20$ dBW, performance gains saturate, indicating that further increases in relay power offer negligible benefit. This saturation behavior is particularly relevant for system design, as it suggests that near-optimal performance can be achieved with moderate ISL power, reducing satellite energy consumption.

Finally notice that even with $P_T = 0$ dBW SSR/MSR maintains a gain of 1-2 dB with respect to HH. This demonstrates that SH not only enhances reliability but also supports low-power satellite designs—a key advantage for large-scale constellations where minimizing onboard energy use is critical.

E. EFFECT OF IMPERFECT CSI

Figure 8 illustrates the impact on BLER performance of imperfect CSI for the proposed SSR and MSR schemes. In the imperfect-CSI case, a pilot-to-symbol power ratio of $E_p = 1$ is assumed, i.e., pilots are transmitted with the same power as data symbols. For comparison, the conventional HH scheme with perfect CSI is also included as a performance benchmark.

As expected, imperfect CSI leads to noticeable performance degradation due to channel estimation errors, which reduce the effectiveness of MRC at the serving satellite. For example, at a 13 dB reference SNR, MSR with perfect CSI achieves a BLER of 10^{-5}, whereas with imperfect CSI, the achieved BLER is around 10^{-4}, clearly showing the sensitivity of MRC performance to CSI accuracy, particularly at higher SNRs. Despite this degradation, SH-SSR with imperfect CSI still outperforms the HH scheme by achieving

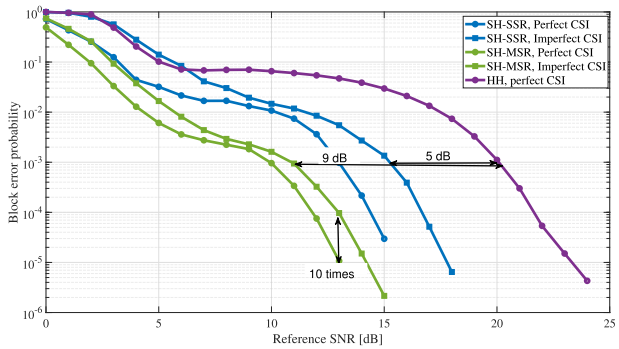

FIGURE 8. Impact of imperfect CSI on BLER performance versus reference SNR for HH, SH-SSR, and SH-MSR schemes under MRC.

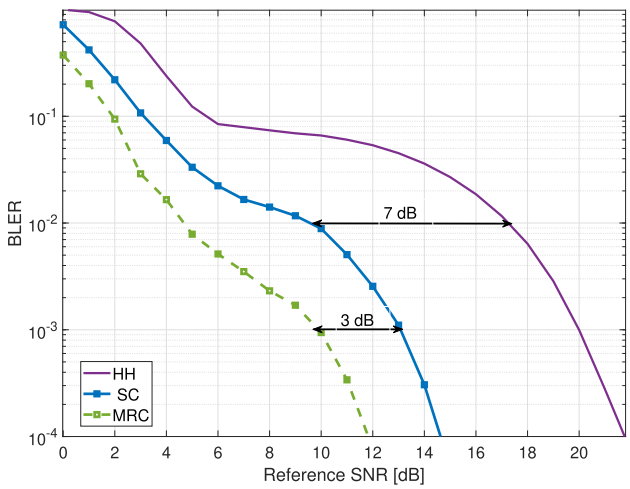

FIGURE 9. BLER performance comparison of SC, MRC, and HH as a function of the reference SNR. For the SH curves, MSR scenario.

the same target BLER 10^{-4} with a gain of 5dB less in needed reference SNR. This result underscores the robustness of cooperative reception, even when CSI is imperfect.

A direct comparison between MSR and SSR further confirms the advantage of spatial diversity, even with imperfect CSI. For a 13 dB reference SNR, MSR achieves a BLER of approximately 10^{-4}, whereas SSR requests 4dB more to achieve the same BLER. These results indicate that MSR, even under imperfect CSI conditions, continues to provide superior Quality of Service (QoS) for the GU. Thus, the additional relay diversity effectively preserves performance and mitigates the impact of channel estimation errors.

F. SC VERSUS MRC

In this subsection, we compare MSR performance under SC and MRC. The corresponding BLER results are presented in Fig. 9. As expected, MRC outperforms SC by about 3 dB at a target BLER equal to 10^{-3}. However, at the same BLER, SC maintains a gain of about 7 dB with respect to plain HH. In other words, SC remains an appealing low-complexity alternative to MRC, retaining most of the diversity benefit while requiring significantly less signal processing and avoiding the need of signal alignment.

In practical terms, MRC should be preferred in systems with stringent BLER requirements and sufficient computational and memory resources, whereas SC offers a well-balanced trade-off between complexity and reliability, making it suitable for scenarios prioritizing simplicity and robustness.

VI. DISCUSSION

The previous section highlighted the relevant performance gain promised by SSR/MSR. In this section, we describe aspects related to the scheme complexity, to the implementation issues, and to the multiuser extension of the work.

A. SSR/MSR COMPLEXITY

Multisatellite reception implies an increase in complexity, from the point-of-view of both computational power and resources allocated. Selecting AF as the relay technique keeps the complexity at the relays to the minimum possible. Substantially, the relaying satellite works as a "bent-pipe" transponder [70], with no signal regeneration. Additionally, each relaying satellite must estimate the G2S channel and forward it to the serving satellite. Most computational burden is on the serving satellite, which needs to combine signals received from one or more neighbor satellites. Notice that MRC and SC scale linearly with the number of relays. Moreover, SC does not even require alignment of the signals received from the different relay satellites.

Regarding resource employment, we can generally say that, if the maximum number of relays is M ($M = 1$ for SSR, while $M > 1$ for MSR), the allocated resources are roughly $M + 1$ times that of single-satellite reception.

In particular, part of the ISL band will be devoted to the transmission of the forwarded signal. With the parameters of Table 5, the ISL has an availability of about 2 THz, while the GU signal has a bandwidth of 5 MHz. If we cautiously suppose that forwarding the relay CSI increases the band occupancy to 100 MHz per GU, this corresponds to the 0.005% of the total band. Even if half of the ISL band is used for other purposes, e.g., to convey a feeder signal from satellites connected to the gateway to satellites that are not [70], the remaining band can still potentially accommodate hundreds or even thousands of GU signals.

If MRC is used, the serving satellite needs to store forwarded messages (with relative CSI information), to align them before combining. To estimate the amount of memory required, we can compute the maximum delay between the signal directly received from the serving satellite and the one coming from the farthest relay satellite. For a given $\delta_{\min}$, the difference between the direct link and the longest G2S link is bounded by

$$\Delta l_{\text{G2S}} \leq h_0 - \sqrt{R_E^2 \sin^2 \delta_{\min} + h_0^2 + 2\, h_0 R_E} + R_E \sin \delta_{\min} \tag{41}$$

which corresponds to about 573 km for $h_0 = 550$ km and $\delta_{\min} = 25°$. To Δl_{G2S} in (41) we must add the length of the IRS link. As an example, for $N_{\text{sat}} = 100$ and $\delta_{\min} = 25°$, the longest ISL connects the serving satellite with its second neighbor, so that the maximum ISL length will be given by

$$\Delta l_{\text{ISL}} = 2\,(R_E + h_0) \sin \frac{2\pi}{N_{\text{sat}}} \approx 870 \text{ km} \tag{42}$$

Hence, the total delay of the latest received relay signal w.r.t. the direct signal can be computed to be about 5 ms, which corresponds to 25,000 symbol transmissions, with our assumptions. Such an amount of storage corresponds to about one codeword, so it does not seem to be impractical.

B. IMPLEMENTATION ISSUES

To start this subsection on practical implementation, we notice that, since SSR/MSR only applies to the uplink, it does not involve any modification of hardware or protocols at the GU side.

An underlying hypothesis is that the AF relays point their directive G2S antennas toward the GU, and their ISL antennas toward the serving satellite. As far as the G2S link is concerned, LEO satellites can use phased arrays to steer multiple beams toward the desired target. To support such beamforming capabilities, we reckon that the number of G2S antennas at the LEO should be roughly increased by a factor of $M + 1$, where M is the maximum number of relays available.[5]

For the ISL link, two intra-orbit inter-satellite optical terminals are already implemented in operating LEO networks between one satellite and its two neighbors [71]. The addition of more inter-satellite terminals between non-neighbor satellites does not seem unrealistic. In alternative, the communication between non-neighbor satellites can be done through multi-hop links that connect only adjacent satellites, with a saving of hardware. Again for $N_{\text{sat}} = 100$ and $\delta_{\min} = 25°$, with multi-hop links the maximum ISL length becomes

$$\Delta l_{\text{ISL,MH}} = 4\,(R_E + h_0) \sin \frac{\pi}{N_{\text{sat}}}, \tag{43}$$

with negligible increase with respect to (42). However, in multi-hop communication, intermediate satellites need to employ more resources, both in terms of power and bandwidth. An evaluation of performance of multi-hop communication between non-neighbor satellites is deferred to future work.

At first glance, latency moderately increases with SSR/MSR. We have seen in Subsection VI-A that, in our default MSR scenario, the delay introduced by relays is on the order of one codeword transmission. We can reasonably state that the latency increase is of the same order of magnitude.

One of the issues with LEO networks is synchronization. Although it is not trivial, because of the high speed of LEO satellites causing a Doppler shift of several tens of kHz, using GNSS positioning and Doppler pre-compensation

[5] However, we have seen in Subsection V-D that with SSR/MSR we can reduce the constellation size and obtain the same performance of the non-cooperative network.

allows timing and frequency synchronization to permit G2S and inter-satellite communication. However, multi-satellite reception and relaying presumably requires more efficient and timely synchronization. An extension of the present work, where we assumed perfect synchronization, will take into account the impact of synchronization algorithms and phase-noise impairment on the performance of SSR/MSR.

C. EXTENSION TO THE MULTIUSER SCENARIO

Although the purpose of this work is to assess the performance of SSR/MSR on a per-GU basis, we provide in this subsection some insight into the applicability of the proposed scheme in a multi-user setting.

In principle, since SSR/MSR is transparent to GUs, there is no need to modify the way in which RRM is performed in the LEO network, with respect to the case of single-satellite reception. Without delving into the details of a protocol, we can sketch how SSR/MSR works at the system level as follows.

- A given satellite acquires the position of each GU it serves, either because it is communicated by the GU itself or because it is provided by the gateway.
- Knowing the geometry of the constellation, it forwards all positions to the relevant neighbor satellites.
- Any neighbor satellite forms a beam toward GUs whose signals it can relay (either all of them or a subset of them, depending on the satellite load or its sensing/beamforming ability).
- Once it has formed the beam, the neighbor satellite sends to the serving satellite the IDs of the GUs whose signal it relays.

The handling of multiuser interference can be done in principle by suitable beamforming, together with typical RRM methods, such as TDMA or NOMA, used also for non-cooperative satellite reception. On the other hand, MSR substantially improves link reliability and enables a drastic reduction of the required GU transmit power (up to 10–12 dB in our simulations), which in an interference-limited system reduces the aggregate uplink interference seen by neighboring satellites and beams.

Notice that, in principle, the proposed schemes can work for an arbitrary multi-orbit Megaconstellation. We limited the performance assessment to the single-orbit case for two reasons: i) in the single-orbit case, the succession of handovers is trivial, while in a Megaconstellation, the user-satellite association is another variable to take into account; ii) assumptions such as perfect synchronization and availability of an ISL are more realistic in the single-orbit scenario than for the Megaconstellation. Nonetheless, the extension to more general constellation geometries is a future direction of research.

VII. CONCLUSION

In this work, we investigated the performance of cooperative uplink reception for LEO networks. The study compared the conventional HH approach with SSR and MSR reception strategies, considering AF or DF relaying techniques, varying relay transmit power, ISL misalignment, imperfect CSI, MRC and SC as combining techniques.

The simulation results reveal several key insights into LEO network performance. Constellation densification alone offers limited benefits under HH conditions, with performance quickly saturating. In contrast, cooperative strategies such as MSR demonstrate strong scalability, achieving up to a 10 dB reduction in the reference SNR on the G2S link required to reach a BLER of 10^{-4}, compared to HH with a 100-satellite constellation under perfect CSI and no misalignment—highlighting the ability to exploit satellite diversity.

Satellite mobility analysis reveals that while larger constellations shorten individual satellite serving times and increase handover frequency, they simultaneously provide a greater number of available relays, thereby enhancing uplink reliability. Furthermore, ISL misalignment is identified as a critical limiting factor for optical links operating at 193 THz. Even small pointing deviations ($\sigma_\ell^2 > 10^{-4}$) can render such high-frequency ISLs ineffective, diminishing the benefits of the MSR scheme. In contrast, lower-frequency ISLs operating around 2 THz demonstrate significantly greater robustness under realistic alignment conditions, although at the cost of a lower capacity. Power scaling results indicate that cooperative reception achieves full diversity benefits with moderate relay transmit power (around 20 dB W), making it energy-efficient and suitable for large constellations. Even under imperfect CSI, MSR/SSR maintains substantial performance advantages over HH. Finally, while MRC offers the best error performance and reliability, SC offers a good compromise between performance and implementation complexity.

Simulation results and considerations on the practical feasibility of MSR/SSR suggest that cooperative reception can be considered a scalable and energy-efficient strategy for future mega-constellations, enabling reliable connectivity even under stringent BLER requirements and realistic system impairments.

APPENDIX

In the appendix, we prove Proposition 1. Let us consider AF. We omit the time index n for brevity. In the hypothesis that ρ_{ISL} is perfectly known and that, according to the approximation that (30) holds, the true channel coefficients satisfy $h_\ell = \hat{h}_\ell + w_\ell$, $\ell \in \mathcal{V}$, with $w_\ell \sim \mathcal{CN}(0, \frac{1}{\rho_\ell E_p})$, we obtain that the average SNR after MRC when s is the transmitted symbol is given by

$$\mathrm{SNR}_{\mathrm{MRC,AF}} = \frac{\rho_{\mathrm{MRC,AF}}^2 |s|^2}{\rho_{\mathrm{MRC,AF}} + \left(\rho_{\mathrm{S}} |\widehat{h}_{\mathrm{S}}|^2 + \sum_{\ell \in \mathcal{R}} \frac{\widetilde{\rho}_\ell^2}{\rho_\ell} |\widehat{h}_\ell|^2\right) \frac{|s|^2}{E_p}} \tag{44}$$

where

$$\rho_{\mathrm{MRC,AF}} = \rho_{\mathrm{S}}|\widehat{h}_{\mathrm{S}}|^2 + \sum_{\ell\in\mathcal{R}} \widetilde{\rho}_\ell |\widehat{h}_\ell|^2 \tag{45}$$

and

$$\widetilde{\rho}_\ell = \frac{\rho_{\mathrm{ISL}}\rho_\ell}{\rho_{\mathrm{ISL}} + q_\ell} < \rho_\ell \tag{46}$$

Without loss of generality, suppose that $1 \in \mathcal{R}$ and $\widetilde{\rho}_1|\widehat{h}_1|^2 > \widetilde{\rho}_\ell|\widehat{h}_\ell|^2$, $\ell \neq 1$. Then, the SNR of SC is given by

$$\mathrm{SNR}_{\mathrm{SC,AF}} = \begin{cases} \dfrac{\rho_{\mathrm{S}}|\widehat{h}_{\mathrm{S}}|^2|s|^2}{1+|s|^2/E_p}, & \text{if } \rho_{\mathrm{S}}|\widehat{h}_{\mathrm{S}}|^2 > \widetilde{\rho}_1|\widehat{h}_1|^2 \\ \dfrac{\widetilde{\rho}_1|\widehat{h}_1|^2|s|^2}{1+\widetilde{\rho}_1|s|^2/(\rho_1 E_p)}, & \text{if } \rho_{\mathrm{S}}|\widehat{h}_{\mathrm{S}}|^2 < \widetilde{\rho}_1|\widehat{h}_1|^2 \end{cases} \tag{47}$$

Now, denote for brevity

$$A_0 = \rho_{\mathrm{S}}|\widehat{h}_{\mathrm{S}}|^2 + \sum_{\ell\in\mathcal{R}\setminus\{1\}} \widetilde{\rho}_\ell|\widehat{h}_\ell|^2,$$

$$\widetilde{A}_0 = \rho_{\mathrm{S}}|\widehat{h}_{\mathrm{S}}|^2 + \sum_{\ell\in\mathcal{R}\setminus\{1\}} \frac{\widetilde{\rho}_\ell^2}{\rho_\ell}|\widehat{h}_\ell|^2 < A_0,$$

and

$$A_1 = \widetilde{\rho}_1|\widehat{h}_1|^2$$

Let us first suppose $\rho_{\mathrm{S}}|\widehat{h}_{\mathrm{S}}|^2 > \widetilde{\rho}_1|\widehat{h}_1|^2$. Then $\mathrm{SNR}_{\mathrm{MRC,AF}} \geq \mathrm{SNR}_{\mathrm{SC,AF}}$ if

$$\frac{(A_0+A_1)^2}{A_0+A_1+\left(\widetilde{A}_0+\frac{\widetilde{\rho}_1}{\rho_1}A_1\right)\frac{|s|^2}{E_p}} \geq \frac{\rho_{\mathrm{S}}|\widehat{h}_{\mathrm{S}}|^2}{1+\frac{|s|^2}{E_p}} \tag{48}$$

But, since $\widetilde{A}_0 < A_0$ and $\widetilde{\rho}_1 < \rho_1$,

$$\frac{(A_0+A_1)^2}{A_0+A_1+\left(\widetilde{A}_0+\frac{\widetilde{\rho}_1}{\rho_1}A_1\right)\frac{|s|^2}{E_p}} > \frac{A_0+A_1}{1+\frac{|s|^2}{E_p}} > \frac{A_0}{1+\frac{|s|^2}{E_p}} \tag{49}$$

so that, since $A_0 > \rho_{\mathrm{S}}|\widehat{h}_{\mathrm{S}}|^2$, (48) follows. Thus, when $\rho_{\mathrm{S}}|\widehat{h}_{\mathrm{S}}|^2 > \widetilde{\rho}_1|\widehat{h}_1|^2$, MRC is always better than SC.

Considering $\rho_{\mathrm{S}}|\widehat{h}_{\mathrm{S}}|^2 < \widetilde{\rho}_1|\widehat{h}_1|^2$, we have $\mathrm{SNR}_{\mathrm{MRC,AF}} \leq \mathrm{SNR}_{\mathrm{SC,AF}}$ if

$$\frac{(A_0+A_1)^2}{A_0+A_1+\left(\widetilde{A}_0+\frac{\widetilde{\rho}_1}{\rho_1}A_1\right)\frac{|s|^2}{E_p}} \leq \frac{A_1}{1+\frac{\widetilde{\rho}_1|s|^2}{\rho_1 E_p}} \tag{50}$$

which, after a little bookkeeping, yields

$$A_0\left(1+\frac{\widetilde{\rho}_1|s|^2}{\rho_1 E_p}\right) \leq A_1\left(\frac{\widetilde{A}_0}{A_0}\frac{|s|^2}{E_p} - 2\frac{\widetilde{\rho}_R|s|^2}{\rho_R E_p} - 1\right) \tag{51}$$

Since $\widetilde{A}_0 < A_0$, if $E_p \geq \max_{s\in\mathcal{S}}|s|^2$, the parenthesis on the RHS of the above equation is negative, and since the LHS is positive, we conclude that $\mathrm{SNR}_{\mathrm{MRC,AF}} \geq \mathrm{SNR}_{\mathrm{SC,AF}}$ always.

The proof for DF goes along the same lines and is omitted.

ACKNOWLEDGMENT

Funded by the European Union, under ANTERRA 101072363 HORIZON-Marie Skłodowska-Curie Actions (MSCA)-2021-Doctoral Network(DN)-01. Views and opinions expressed are however those of the authors only and do not necessarily reflect those of the European Union. Neither the European Union nor the granting authority can be held responsible for them.

REFERENCES

[1] U. Gustavsson, P. Frenger, C. Fager, T. Eriksson, H. Zirath, F. Dielacher, C. Studer, A. Pärssinen, R. Correia, J. N. Matos, D. Belo, and N. B. Carvalho, "Implementation challenges and opportunities in beyond-5G and 6G communication," *IEEE J. Microw.*, vol. 1, no. 1, pp. 86–100, Jan. 2021.

[2] N. Rajatheva et al., "Scoring the terabit/s goal: Broadband connectivity in 6G," Tech. Rep., 2021. [Online]. Available: https://arxiv.org/abs/2008.07220

[3] M. Tropea and F. De Rango, "A comprehensive review of channel modeling for land mobile satellite communications," *Electronics*, vol. 11, no. 5, p. 820, Mar. 2022.

[4] E. Juan, M. Lauridsen, J. Wigard, and P. Mogensen, "Handover solutions for 5G low-Earth orbit satellite networks," *IEEE Access*, vol. 10, pp. 93309–93325, 2022.

[5] Y.-H. Chu, C.-W. Cho, and M.-S. Pan, "An effective handover strategy for fast-moving devices in LEO satellite network based on deep reinforcement learning," in *Proc. Int. Conf. Inf. Netw. (ICOIN)*, Jan. 2025, pp. 369–373.

[6] C. Loo, "A statistical model for a land mobile satellite link," *IEEE Trans. Veh. Technol.*, vol. VT-34, no. 3, pp. 122–127, Aug. 1985.

[7] Y. Lee and J. P. Choi, "Performance evaluation of high-frequency mobile satellite communications," *IEEE Access*, vol. 7, pp. 49077–49087, 2019.

[8] G. E. Corazza and F. Vatalaro, "A statistical model for land mobile satellite channels and its application to nongeostationary orbit systems," *IEEE Trans. Veh. Technol.*, vol. 43, no. 3, pp. 738–742, Mar. 1994.

[9] G. E. Corazza, C. Ferrarelli, and F. Vatalaro, "A rice-lognormal terrestrial and satellite channel model," in *Proc. 3rd IEEE Int. Conf. Universal Pers. Commun.*, Mar. 1994, pp. 155–159.

[10] Y. Xie and Y. Fang, "A general statistical channel model for mobile satellite systems," *IEEE Trans. Veh. Technol.*, vol. 49, no. 3, pp. 744–752, May 2000.

[11] E. Lutz, D. Cygan, M. Dippold, F. Dolainsky, and W. Papke, "The land mobile satellite communication channel-recording, statistics, and channel model," *IEEE Trans. Veh. Technol.*, vol. 40, no. 2, pp. 375–386, May 1991.

[12] E. Lutz, "A Markov model for correlated land mobile satellite channels," *Int. J. Satell. Commun.*, vol. 14, no. 4, pp. 333–339, Jul. 1996.

[13] S. Rougerie, F. Lacoste, and B. Montenegro-Villacieros, "Mobile satellite propagation channels for Ku and Ka band," in *Proc. 10th Eur. Conf. Antennas Propag. (EuCAP)*, Montenegro, Apr. 2016, pp. 1–5.

[14] A. O. Akinniyi, A. T. Tola, and O. Olatunde, "Modelling of land mobile satellite channel to counter channel outage," *Int. J. Distrib. Parallel Syst.*, vol. 8, no. 2, pp. 1–21, Mar. 2017.

[15] L. Bai, C.-X. Wang, G. Goussetis, S. Wu, Q. Zhu, W. Zhou, and E.-H.-M. Aggoune, "Channel modeling for satellite communication channels at Q-band in high latitude," *IEEE Access*, vol. 7, pp. 137691–137703, 2019.

[16] L. E. Braten and T. Tjelta, "Semi-Markov multistate modeling of the land mobile propagation channel for geostationary satellites," *IEEE Trans. Antennas Propag.*, vol. 50, no. 12, pp. 1795–1802, Dec. 2002.

[17] Y. Karasawa, K. Kimura, and K. Minamisono, "Analysis of availability improvement in LMSS by means of satellite diversity based on three-state propagation channel model," *IEEE Trans. Veh. Technol.*, vol. 46, no. 4, pp. 1047–1056, Apr. 1997.

[18] F. P. Fontan, M. Vazquez-Castro, C. E. Cabado, J. P. Garcia, and E. Kubista, "Statistical modeling of the LMS channel," *IEEE Trans. Veh. Technol.*, vol. 50, no. 6, pp. 1549–1567, Jun. 2001.

[19] M. Milojevic, M. Haardt, E. Eberlein, and A. Heuberger, "Channel modeling for multiple satellite broadcasting systems," *IEEE Trans. Broadcast.*, vol. 55, no. 4, pp. 705–718, Dec. 2009.

[20] T. Liu, B. Sun, Z. Li, and Z. Dou, "Analysis of channel characteristics and channel model for satellite communication system," in *Proc. IEEE Int. Conf. Electron. Inf. Commun. Technol. (ICEICT)*, Aug. 2016, pp. 166–169.

[21] D. Rey Iglesias and M. Garcia Sanchez, "Semi-Markov model for low-elevation satellite–Earth radio propagation channel," *IEEE Trans. Antennas Propag.*, vol. 60, no. 5, pp. 2481–2490, May 2012.

[22] M. Yan, Y. Dou, and B. Xie, "Statistical modeling of land mobile satellite dual-polarized MIMO propagation channel," in *Proc. Int. Symp. Netw., Comput. Commun. (ISNCC)*, Oct. 2021, pp. 1–5.

[23] H. Ming, S. Dongya, C. Yanni, X. Jie, Y. Dong, C. Jie, and L. Anxian, "A new five-state Markov model for land mobile satellite channels," in *Proc. 8th Int. Symp. Antennas, Propag. EM Theory*, 2008, pp. 1512–1515.

[24] D. Shen, J. Rong, Y. Yang, Y. Guo, H. Cao, and S. Fu, "The six-state Markov model for land mobile satellite channels," in *Proc. IEEE Int. Symp. Microw., Antenna, Propag. EMC Technol. Wireless Commun.*, vol. 2, May 2005, pp. 1619–1622.

[25] H. Ming, S. Dongya, C. Yanni, X. Jie, and Z. Cuiqing, "Theoretical analysis and simulation of the outage probability for six-state Markov model on land-mobile satellite channels," in *Proc. 8th Int. Symp. Antennas, Propag. EM Theory*, 2008, pp. 1516–1519.

[26] F. Babich and G. Lombardi, "A Markov model for the mobile propagation channel," *IEEE Trans. Veh. Technol.*, vol. 49, no. 1, pp. 63–73, Jan. 2000.

[27] J.-C. Hsieh, H.-P. Lin, and C. Yang, "A two-level, multi-state Markov model for satellite propagation channels," in *Proc. IEEE VTS 53rd Veh. Technol. Conf., Spring*, vol. 4, Jan. 2001, pp. 3005–3009.

[28] Q. Zhang and S. A. Kassam, "Finite-state Markov model for Rayleigh fading channels," *IEEE Trans. Commun.*, vol. 47, no. 11, pp. 1688–1692, Nov. 1999.

[29] M. Tropea, P. Fazio, F. Veltri, and S. Marano, "Markovian channel modeling for DVB-RCS satellite systems based on observation window concept," in *Proc. 9th Int. Wireless Commun. Mobile Comput. Conf. (IWCMC)*, Jul. 2013, pp. 736–740.

[30] M. Tropea, P. Fazio, F. Veltri, and S. Marano, "A new DVB-RCS satellite channel model based on discrete time Markov chain and quality degree," in *Proc. IEEE Wireless Commun. Netw. Conf. (WCNC)*, Apr. 2013, pp. 2615–2619.

[31] H. Shen Wang and N. Moayeri, "Finite-state Markov channel—A useful model for radio communication channels," *IEEE Trans. Veh. Technol.*, vol. 44, no. 1, pp. 163–171, Feb. 1995.

[32] J. Restrepo and G. Maral, "Coverage concepts for satellite constellations providing communications services to fixed and mobile users," *Space Commun.*, vol. 13, no. 2, pp. 145–157, 1995.

[33] Z. Liu, Z. Yang, G. Pan, H. Zhang, G. Luo, and H. Yang, "Handover technique in LEO satellite networks: A review," in *Proc. 13th Int. Conf. Commun., Circuits Syst. (ICCCAS)*, May 2024, pp. 364–369.

[34] P. Chowdhury, M. Atiquzzaman, and W. Ivancic, "Handover schemes in satellite networks: State-of-the-art and future research directions," *IEEE Commun. Surveys Tuts.*, vol. 8, no. 4, pp. 2–14, 2006.

[35] M. I. Mughal, "Analysis of handover queuing schemes in mobile satellite systems of Earth's lower orbit," in *Proc. 2nd Nat. Conf. Space ScienceAt*. HEJ Auditorium, University of Karachi, Jan. 2013. [Online]. Available: https://www.researchgate.net/publication/273126799_Analysis_of_Handover_Queuing_Schemes_in_Mobile_Satellite_Systems_of_Earth's_Lower_Orbit

[36] J. Miao, P. Wang, H. Yin, N. Chen, and X. Wang, "A multi-attribute decision handover scheme for LEO mobile satellite networks," in *Proc. IEEE 5th Int. Conf. Comput. Commun. (ICCC)*, Dec. 2019, pp. 938–942.

[37] S. Karapantazis and F.-N. Pavlidou. (2005). *Design Issues and QoS Handover Management for Broadband Leo Satellite Systems*. [Online]. Available: https://api.semanticscholar.org/CorpusID:55108862

[38] G. Giambene, *Resource Management in Satellite Networks: Optimization and Cross-Layer Design*. New York, NY, USA: Springer, 2007.

[39] H. Uzunalioglu, "Probabilistic routing protocol for low Earth orbit satellite networks," in *Proc. ICC 98th IEEE Int. Conf. Communications. Conf. Record. Affiliated SUPERCOMM*, vol. 1, Feb. 1998, pp. 89–93.

[40] H. Liu, Y. Wang, P. Li, and J. Cheng, "A multi-agent deep reinforcement learning-based handover scheme for mega-constellation under dynamic propagation conditions," *IEEE Trans. Wireless Commun.*, vol. 23, no. 10, pp. 13579–13596, Oct. 2024.

[41] Y. Su, Y. Liu, Y. Zhou, J. Yuan, H. Cao, and J. Shi, "Broadband LEO satellite communications: Architectures and key technologies," *IEEE Wireless Commun.*, vol. 26, no. 2, pp. 55–61, Apr. 2019.

[42] S. Karapantazis and P. Todorova. (2005). *On Call Admission Control and Handover Management in Multimedia Leo Satellite Systems*. [Online]. Available: https://api.semanticscholar.org/CorpusID:14799506

[43] H. B. Salem, A. Tarable, A. Nordio, and B. Makki, "Uplink soft handover for LEO constellations: How strong the inter-satellite link should be," in *Proc. IEEE 35th Int. Symp. Pers., Indoor Mobile Radio Commun. (PIMRC)*, Sep. 2024, pp. 1–7.

[44] S. Nie and I. F. Akyildiz, "Channel modeling and analysis of inter-small-satellite links in terahertz band space networks," *IEEE Trans. Commun.*, vol. 69, no. 12, pp. 8585–8599, Dec. 2021.

[45] A. Masihi, P. Testolina, and J. M. Jornet, "Terahertz vs. Optical for inter-satellite links: A comparative analysis of pointing errors and system performance," in *Proc. IEEE Int. Conf. Commun. Workshops (ICC Workshops)*, Jun. 2025, pp. 964–970.

[46] K. Dasala, "Mobile terahertz inter-small-satellite links with angular dispersion," in *Proc. 23rd Int. Symp. Model. Optim. Mobile, Ad Hoc, Wireless Netw.*, May 2025, pp. 1–8.

[47] W. Gao, Z. Yang, and C. Han, "Channel modeling and evaluation on terahertz orbital angular momentum (OAM)-based intersatellite communications," *IEEE Trans. Antennas Propag.*, vol. 73, no. 7, pp. 4840–4852, Jul. 2025.

[48] J. Lyu, Y. L. Guan, X. Liu, and E. Gunawan, "Inter-orbital inter-satellite communication link performance analysis at THz band considering gravity-induced antenna pointing error," *IEEE Trans. Veh. Technol.*, vol. 74, no. 6, pp. 10000–10005, Jun. 2025.

[49] Z. Wu, F. Jin, J. Luo, Y. Fu, J. Shan, and G. Hu, "A graph-based satellite handover framework for LEO satellite communication networks," *IEEE Commun. Lett.*, vol. 20, no. 8, pp. 1547–1550, Aug. 2016.

[50] S. Zhang, A. Liu, C. Han, X. Ding, and X. Liang, "A network-flows-based satellite handover strategy for LEO satellite networks," *IEEE Wireless Commun. Lett.*, vol. 10, no. 12, pp. 2669–2673, Dec. 2021.

[51] Y. Cao, S.-Y. Lien, and Y.-C. Liang, "Deep reinforcement learning for multi-user access control in non-terrestrial networks," *IEEE Trans. Commun.*, vol. 69, no. 3, pp. 1605–1619, Mar. 2021.

[52] Y. Wu, G. Hu, F. Jin, and J. Zu, "A satellite handover strategy based on the potential game in LEO satellite networks," *IEEE Access*, vol. 7, pp. 133641–133652, 2019.

[53] P.-D. Arapoglou, K. Liolis, M. Bertinelli, A. Panagopoulos, P. Cottis, and R. De Gaudenzi, "MIMO over satellite: A review," *IEEE Commun. Surveys Tuts.*, vol. 13, no. 1, pp. 27–51, 1st Quart., 2011.

[54] R. T. Schwarz, T. Delamotte, K.-U. Storek, and A. Knopp, "MIMO applications for multibeam satellites," *IEEE Trans. Broadcast.*, vol. 65, no. 4, pp. 664–681, Dec. 2019.

[55] R. Richter, I. Bergel, Y. Noam, and E. Zehavi, "Downlink cooperative MIMO in LEO satellites," *IEEE Access*, vol. 8, pp. 213866–213881, 2020.

[56] L. You, K.-X. Li, J. Wang, X. Gao, X.-G. Xia, and B. Ottersten, "Massive MIMO transmission for LEO satellite communications," *IEEE J. Sel. Areas Commun.*, vol. 38, no. 8, pp. 1851–1865, Aug. 2020.

[57] Z. Xiang, X. Gao, K.-X. Li, and X.-G. Xia, "Massive MIMO downlink transmission for multiple LEO satellite communication," *IEEE Trans. Commun.*, vol. 72, no. 6, pp. 3352–3364, Jun. 2024.

[58] X. Zhang, S. Sun, M. Tao, Q. Huang, and X. Tang, "Multi-satellite cooperative networks: Joint hybrid beamforming and user scheduling design," *IEEE Trans. Wireless Commun.*, vol. 23, no. 7, pp. 7938–7952, Jul. 2024.

[59] *Propagation Data Required for the Design of Systems in the Land Mobile-satellite Service*, document TU-R P.681-11, Aug. 2019. [Online]. Available: https://www.itu.int/rec/R-REC-P.681-11-201908-I/en

[60] M. Richharia and L. Westbrook, *Satellite Systems for Personal Applications: Concepts and Technology* (Wireless Communications and Mobile Computing). Hoboken, NJ, USA: Wiley, 2010. [Online]. Available: https://books.google.it/books?id=TC1KZTaCLU8C

[61] Wikipedia contributors. (2025). *Atan2—Wikipedia, The Free Encyclopedia*. [Online]. Available: https://en.wikipedia.org/wiki/Atan2

[62] L. M. Kells, W. F. Kern, and J. R. Bland, *Plane and Spherical Trigonometry*. New York, NY, USA: McGraw-Hill, 1940.

[63] *3rd Generation Partnership Project; Technical Specification Group Radio Access Network: Study on New Radio (NR) To Support Nonterrestrial Networks*, document 3GPP TR 38.811, 3GPP, Jun. 2018.

[64] J. M. Romero-Jerez, F. J. Lopez-Martinez, J. F. Paris, and A. J. Goldsmith, "The fluctuating two-ray fading model: Statistical characterization and performance analysis," *IEEE Trans. Wireless Commun.*, vol. 16, no. 7, pp. 4420–4432, Jul. 2017.

[65] J. D. V. Sánchez, F. J. Lopez-Martinez, J. F. Paris, and J. M. Romero-Jerez, "The multi-cluster fluctuating two-ray fading model," *IEEE Trans. Wireless Commun.*, vol. 23, no. 5, pp. 4199–4213, May 2024.

[66] D. Tse and P. Viswanath, *Fundamentals of Wireless Communication*. Cambridge, U.K.: Cambridge Univ. Press, 2005.

[67] F. I. G. Carvalho, R. V. d. O. Paiva, T. F. Maciel, V. F. Monteiro, F. R. M. Lima, D. C. Moreira, D. A. Sousa, B. Makki, M. Åström, and B. Lei, "Network-controlled repeater—An introduction," *IEEE Commun. Standards Mag.*, vol. 10, no. 1, pp. 186–193, Jan. 2024.

[68] T. Richardson and R. Urbanke, *Modern Coding Theory*. Cambridge, U.K.: Cambridge Univ. Press, 2008.

[69] T. Cover and J. Thomas, *Elements of Information Theory* (Wiley Series in Telecommunications and Signal Processing). Hoboken, NJ, USA: Wiley, 1991. [Online]. Available: https://books.google.se/books?id=CX9QAAAAMAAJ

[70] J. Zheng, T. H. Luan, G. Li, J. Zhao, Z. Yin, N. Cheng, and J. Pan, "Low Earth orbit satellite networks: Architecture, key technologies, measurement, and open issues," *IEEE Netw.*, vol. 40, no. 2, pp. 295–303, Feb. 2025.

[71] N. Benso, A. Compagnoni, G. F. Stock, J. A. Fraire, G. M. Capez, C. Ottaviani, D. G. Riviello, G. Verardo, M. Gargiulo, L. Ospizio, C. F. Chiasserini, and R. Garello, "Distributed on-demand routing for VLEO constellations with 3-terminal inter-satellite links," in *Proc. Int. Conf. Softw., Telecommun. Comput. Netw. (SoftCOM)*, Sep. 2025, pp. 1–7.

HOUCEM BEN SALEM received the Multidisciplinary Engineering degree from the École Polytechnique de Tunisie, Tunis, Tunisia. He is currently pursuing the Ph.D. degree in electrical, electronics, and communications engineering with the Politecnico di Torino, Turin, Italy, as part of the Marie Skłodowska-Curie Research Program. As part of his doctoral work, he spent 1.5 years as a Researcher with CNR-IEIIT, Turin, and is completing the final 1.5 years of his research with Ericsson, Gothenburg, Sweden. His current research interests include satellite communications, inter-satellite links, signal processing, synchronization techniques, and beyond 5G systems.

BEHROOZ MAKKI (Senior Member, IEEE) received the Ph.D. degree in communication engineering from the Chalmers University of Technology, Gothenburg, Sweden. He was a Postdoctoral Researcher with the Chalmers University of Technology, from 2013 to 2017. He is currently a Senior Researcher with Ericsson Research, Gothenburg. He has co-authored more than 75 journal articles, more than 60 conference papers, and more than 250 patent applications. His current research interests include integrated access and backhaul, green communications, millimeter wave communications, NOMA, and backhauling. He is an Editor of IEEE Transactions on Communications and IEEE Transactions on Wireless Communications and a Senior Editor of IEEE Wireless Communications Letters and IEEE Communications Letters. He has been selected as an IEEE Distinguished Lecturer, in 2025.

ALBERTO TARABLE (Member, IEEE) received the Laurea degree (summa cum laude) and the Ph.D. degree in electronic engineering from the Politecnico di Torino, in 1998 and February 2002, respectively. From 2002 to 2012, he was a Postdoctoral Researcher with the Department of Electronics and Telecommunications, Politecnico di Torino. He has been a Researcher (since 2012) and a Senior Researcher (since 2023) with the Institute of Electronics, Computer and Telecommunication Engineering, Italian National Research Council. He has co-authored more than 80 papers on international journals and conferences. His research interests include physical-layer design of communication systems, NTN, and QKD systems.